Available online at www.sciencedirect.com
ScienceDirect
Journal of Sound and Vibration 302 (2007) 657–682
JOURNAL OF SOUND AND VIBRATION
www.elsevier.com/locate/jsvi

Autoparametric resonances in elastic structures carrying two rectangular tanks partially filled with liquid

Takashi Ikeda*

Department of Electronic and Control Systems Engineering, Shimane University, 1060 Nishikawatsu, Matsue 690-8504, Japan

Received 30 October 2005; received in revised form 4 October 2006; accepted 13 November 2006
Available online 27 February 2007

Abstract

Nonlinear vibrations of elastic structures carrying two liquid-filled tanks under vertical harmonic excitation are investigated. A 2:1:1 ratio of internal resonance is satisfied between the natural frequency of the structure and the lowest natural frequencies of sloshing in two rectangular liquid tanks. The theoretical analysis here is restricted to two-dimensional flow and three-dimensional Faraday waves are not considered. The finite fluid depths are also assumed. Modal equations of motion are derived by using Galerkin's method, taking into account the nonlinearity of the hydrodynamic force. Then, frequency response curves are determined by using van der Pol's method. The respective influences of the liquid levels and the deviation of the internal resonance ratio (i.e., the mistuning) on the frequency response curves are demonstrated. As a result, we have obtained results different from those obtained in the case of a structure with a single liquid-filled tank. It is found that two types of vibrations can occur depending on the liquid levels and the excitation frequency: a single-mode solution (sloshing in either tank) and a double-mode solution (sloshing in both tanks). Amplitude- and phase-modulated motion including chaotic vibrations appears on the branches of the frequency response curves, which correspond to the single mode solution, when some deviation of the internal resonance ratio exists. The validity of the theoretical results was verified by the experiments.

1. Introduction

Vibration suppression in elastic structures such as elevated water tanks and liquefied natural gas (LNG) storage tanks is one of the most important issues in engineering. Tuned liquid dampers (TLDs) were devised as a countermeasure of the vibration suppression, utilizing the liquid force due to liquid sloshing. Therefore, it is necessary to comprehend the dynamic behavior of sloshing in order to design the TLD with high performance. Until now, many papers regarding this topic have been reviewed in Ref. [1]. At the beginning of the study on the TLD, the linear analysis was conducted by Senda and Nakagawa [2]. However, the linear analysis is no longer valid when large amplitude waves are generated on a liquid free surface, because the nonlinear effects due to liquid inertia become significant. Therefore, no analytical results with high accuracy can be obtained without considering the nonlinear effects of the fluid forces. Studies on the nonlinear analysis of sloshing in

*Tel.: +81 852 32 8908; fax: +81 852 32 8909.
E-mail address: tikeda@riko.shimane-u.ac.jp.

0022-460X/$ - see front matter © 2007 Elsevier Ltd. All rights reserved.
doi:10.1016/j.jsv.2006.11.037

Nomenclature

c	damping coefficient of the structure
d_1, d_2	widths of tanks 1 and 2, respectively
F_1, F_2	vertical fluid forces from tanks 1 and 2, respectively
F_0	amplitude of harmonic excitation
g	acceleration of gravity
h_1, h_2	liquid levels (or depths) in tanks 1 and 2, respectively
k	spring constant of the structure
M	summation of masses of the structure and the liquid ($=m+m_1+m_2$)
m	mass of the structure
m_1, m_2	masses of the liquid in tanks 1 and 2, respectively
P_1, P_2	fluid pressures in tanks 1 and 2, respectively
p_0	natural frequency of the structure
p_n	natural frequency of the nth sloshing mode (n: integer)
l	tank length
t	time
(x_i, y_i, z_i)	rectangular coordinate system (see Fig. 1)
z_0	vertical displacement of the structure
η_1, η_2	elevations of the liquid surfaces in tanks 1 and 2, respectively
v	$=m/M$
ρ	fluid density
ϕ_1, ϕ_2	velocity potentials of fluid in tanks 1 and 2, respectively
ω	excitation frequency
ζ_n, $\bar{\zeta}_n$	damping ratios of nth sloshing modes in tanks 1 and 2, respectively
*	dimensional parameter

liquid tanks have been developed rapidly by Hutton [3] and Abramson [4] for a horizontal excitation, as well as Skalak and Yarymovych [5] and Dodge et al. [6] for a vertical excitation. Standing waves that appear on liquid surface in a vertically vibrating container are referred to as Faraday waves [7]. Henderson and Miles [8] experimentally investigated them for the 2:1 internal resonance in a circular cylinder. Miles [9,10] theoretically analyzed them for three-dimensional waves. Fultz [11] showed experimentally that the frequency response curves changed from a soft spring type to a hard spring type as a liquid level decreased in a rectangular tank subjected to horizontal excitation. Ockendon and Ockendon [12], Hayama et al. [13] and Faltinsen et al. [14] theoretically showed the passage from a soft type to a hard type and the critical liquid level. In addition, Waterhouse [15] analyzed the resonance near the critical liquid level. When the liquid level was furthermore lower, Faltinsen and Timokha [16] and Hill [17] investigated sloshing dynamics as shallow water. Recently, Hill and Frandsen [18] compared the analytical results of the transient evolution of the wave amplitude in a rectangular tank subjected to horizontal excitation with computational results. Bredmose et al. [19] reported on the comparison of experimental and numerical results of steep forced water waves in a rectangular tank subjected to horizontal or vertical excitation.

Most of the TLDs have been studied on elastic structures subjected to a horizontal excitation. This can be inferred by considering that seismic vibrations and wind-induced vibrations of buildings fall into the category of the horizontal excitation. First, this kind of study can be briefly summarized as follows: Modi and Welt [20] devised a torus-shaped nutation damper and they adopted the perturbation method similar to one used by Hutton [3] to compare the theoretical results with the experimental results. Fujino et al. [21] used a rectangular liquid tank to investigate the effectiveness of the TLD by the numerical simulation using a nonlinear finite-difference scheme. Also, more practical TLDs have been developed. For example, Hagiuda [22] applied the TLD, which was a rectangular tank with submerged nets, to pylons of cable-stayed bridges. Tamura et al. [23] developed the TLD which was applied to towers and high-rise buildings subjected to wind excitation. The author of the present paper used Galerkin's method to investigate nonlinear vibrations in structure/fluid interaction systems and he obtained the theoretical results coincident with the experimental data [24,25]. Kaneko and Yoshida [26] conducted a nonlinear analysis by using Galerkin's method to estimate the effectiveness of the TLD developed by Hagiuda. Even now, this kind of study is continuing. Frandsen [27] investigated the TLD's performance using a finite-difference time-stepping scheme on adaptively mapped grids.

On the other hand, elastic structures subjected to a vertical excitation can be seen in roads on long suspension bridges, transmission wires and street light poles. However, the dynamic responses of the TLD

under a vertical excitation have rarely been investigated. Ibrahim and Barr [28] considered only one sloshing mode in a cylindrical tank to conduct a nonlinear analysis, and hence their results did not sufficiently agree with the experimental data. The author of the present paper obtained the theoretical results, which agreed well with the experimental data, taking into account the adequate number of sloshing modes for a rectangular tank [29] as well as a cylindrical tank [30].

Most of this research has investigated the behavior of the structure carrying just one liquid tank subjected to horizontal excitation or vertical excitation. However, considering that multiple liquid tanks are commonly used in practical systems, it seems necessary to investigate the performance of the TLD with multiple liquid tanks.

The present paper deals with an elastic structure, carrying two liquid-filled rectangular tanks and being subjected to a vertical sinusoidal excitation. The internal resonance ratio 2:1:1 holds between the natural frequency of the structure and the lowest natural frequencies of sloshing in the two tanks. The theoretical analysis here is restricted to two-dimensional flow and three-dimensional Faraday waves are not considered. The finite fluid depths are also assumed. The nonlinearity of the hydrodynamic force is considered and the modal equations governing this system are derived. Then, the theoretical frequency response curves are calculated by using van del Pol's method [31], which shows that they are influenced significantly by the excitation frequency, the liquid level and the deviation of the internal resonance ratio. In addition, the performance of the TLD with two liquid tanks is described. The validity of the theoretical results was verified by the experiments.

2. Theoretical analysis

2.1. Equations of motion

Fig. 1 shows the theoretical model. A general mechanical structure is modeled as a single-degree-of-freedom (sdof) system, which consists of the mass m, the spring with spring constant k^*, and the dashpot with damping coefficient c^*. This structure is subjected to a vertical sinusoidal excitation $F_0^*\cos\omega^* t^*$. Two rectangular liquid-filled tanks with a length l^*, called tanks 1 and 2, are mounted on the structure. Hereinafter, the symbols denoting the system parameters have a subscript 'i' to distinguish between tank 1 and tank 2. The tanks of the cross areas $l^* \times d_i^*$ are partially filled with liquid to depths h_i^*. It should be noted that the 1:1-sloshing resonance implies $h_1^* \approx h_2^*$ for the liquid depths, because the two tanks have an identical length l^*. In Fig. 1, the coordinate systems O_i-$x_i^* y_i^* z_i^*$ moving together with the tanks are considered. The planes $x_i^* y_i^*$ are chosen as the liquid free surfaces at rest. The liquid motion is assumed possible in the $x_i^* z_i^*$ planes. The vertical displacement of the

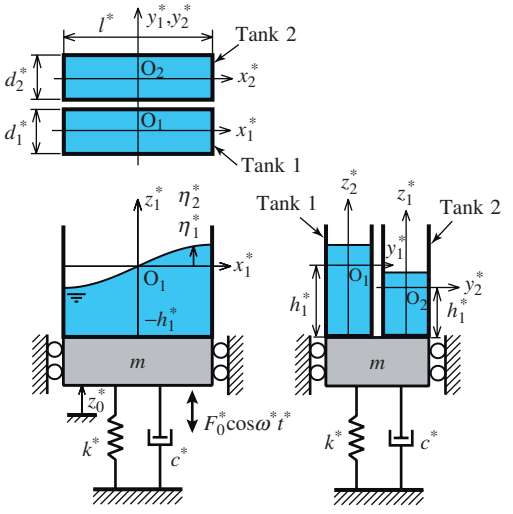

Fig. 1. Model for theoretical analysis.

structure, measured from its equilibrium position, is z_0*. The elevations of the liquid surfaces at the position x_i* are η_i*. Here, the velocity potential ϕ_i* of the liquid particles, moving relative to the tanks, are introduced by using potential flow theory. Laplace's equations (i.e., the continuity equations) are given in terms of ϕ_i*:

$$\Delta\phi_i^*(x_i^*, z_i^*, t^*) \equiv \frac{\partial^2\phi_i^*}{\partial x_i^{*2}} + \frac{\partial^2\phi_i^*}{\partial z_i^{*2}} = 0 \tag{1}$$

and generalized Bernoulli's equations (i.e., the pressure equations) are given in Ref. [16] as

$$\frac{\partial\phi_i^*}{\partial t^*} + \frac{1}{2}\left\{\left(\frac{\partial\phi_i^*}{\partial x_i^*}\right)^2 + \left(\frac{\partial\phi_i^*}{\partial z_i^*}\right)^2\right\} + gz_i^* + \frac{P_i^*}{\rho} = -\ddot{z}_0^* z_i^*, \tag{2}$$

where P_i*(x_i*, z_i*, t*) are the fluid pressures, ρ is the fluid density, g is the acceleration of gravity and the symbol '$\cdot$' represents the derivative with respect to the time t*.

The equation of motion for the structure is

$$m\ddot{z}_0^* + c^*\dot{z}_0^* + k^* z_0^* = F_1^* + F_2^* + F_0^* \cos\omega^* t^* + m_1 g + m_2 g, \tag{3}$$

where F_i* are the fluid forces acting in the z_i* directions to the structure through the tank bottoms, and m_i are the masses of liquid. The fourth and fifth terms on the right side of Eq. (3) are produced because of the definition of the equilibrium position of z_0*. The fluid forces F_i* are given by

$$F_i^* = -d_i^* \int_{-l^*/2}^{l^*/2} P_i^*(x_i^*, z_i^*, t^*)\big|_{z_i^* = -h_i^*}\, \mathrm{d}x_i^*, \tag{4}$$

where P_i*(x_i*, z_i*, t*) are given by Eq. (2).

Here, the following dimensionless quantities are defined as

$$\begin{aligned} &z_0 = z_0^*/l^*,\ \ \eta_i = \eta_i^*/l^*,\ \ x_i = x_i^*/l^*,\ \ z_i = z_i^*/l^*,\ \ h_i = h_i^*/l,\ \ d_i = \rho d_i^* l^{*2}/M,\ \ v = m/M,\\ &k = k^*/(Mp_1^2),\ \ c = c^*/(Mp_1),\ \ \phi_i = \phi_i^*/l^{*2}p_1,\ \ F_0 = F_0^*/(Ml^*p_1^2),\ \ F_i = F_i^*/(Ml^*p_1^2),\\ &P_i = P_i^*/(\rho l^{*2}p_1^2),\ \ \lambda_n = \lambda_n^* l^* = n\pi,\ \ \omega = \omega^*/p_1,\ \ \omega_n = p_n/p_1,\ \ \bar{\omega}_n = \bar{p}_n/p_1,\ \ t = p_1 t^*, \end{aligned} \tag{5}$$

where

$$M = m + m_1 + m_2,\ \ p_n = \sqrt{g\lambda_n^* \tanh(\lambda_n^* h_1^*)},\ \ \bar{p}_n = \sqrt{g\lambda_n^* \tanh(\lambda_n^* h_2^*)},\ \ \lambda_n^* = n\pi/l^*. \tag{6}$$

In Eq. (6), M is a summation of the masses of the structure and the liquid. p_n and $\bar{p}_n$ represent the nth natural frequencies of sloshing in tanks 1 and 2, respectively. λ_n^* represents the nth characteristic root. Applying Eq. (5) to Eqs. (1)–(4) to be written in a dimensionless form yields

$$\Delta\phi_i(x_i, z_i, t) \equiv \frac{\partial^2\phi_i}{\partial x_i^2} + \frac{\partial^2\phi_i}{\partial z_i^2} = 0, \tag{7}$$

$$\frac{\partial\phi_i}{\partial t} + \frac{1}{2}\left\{\left(\frac{\partial\phi_i}{\partial x_i}\right)^2 + \left(\frac{\partial\phi_i}{\partial z_i}\right)^2\right\} + \frac{z_i}{\psi_1} + P_i = -\ddot{z}_0 z_i, \tag{8}$$

$$v\ddot{z}_0 + c\dot{z}_0 + kz_0 = F_1 + F_2 + F_0 \cos\omega t + d_1 h_1/\psi_1 + d_2 h_2/\psi_1, \tag{9}$$

$$F_i = -d_i \int_{-1/2}^{1/2} P_i(x_i, z_i, t)\big|_{z_i = -h_i}\, \mathrm{d}x_i, \tag{10}$$

where $\psi_1 = \lambda_1 \tanh(\lambda_1 h_1)$.

Because the fluid velocities vanish at the side walls and bottoms of the tanks, the boundary conditions for ϕ_i are given by

$$\frac{\partial\phi_i}{\partial x_i} = 0\ \ (\text{at}\ \ x_i = \pm 1/2), \quad \frac{\partial\phi_i}{\partial z_i} = 0\ \ (\text{at}\ \ z_i = -h_i). \tag{11}$$

Next, because the vertical velocities of the fluid particle at the liquid surface are equal to the velocities of the liquid surfaces in the vertical direction, one can obtain the kinematic boundary conditions [28]

$$\frac{\partial \phi_i}{\partial z_i} = \frac{\partial \eta_i}{\partial t} + \frac{\partial \phi_i}{\partial x_i}\frac{\partial \eta_i}{\partial x_i} \quad (\text{at } z_i = \eta_i). \tag{12}$$

Moreover, because $P_i = 0$ at the free surfaces $z_i = \eta_i$, the boundary conditions for Eq. (8) are given by

$$\frac{\partial \phi_i}{\partial t} + \frac{1}{2}\left\{\left(\frac{\partial \phi_i}{\partial x_i}\right)^2 + \left(\frac{\partial \phi_i}{\partial z_i}\right)^2\right\} + \frac{z_i}{\psi_1} = -\ddot{z}_0 z_i \quad (\text{at } z_i = \eta_i). \tag{13}$$

2.2. Modal equations of motion

In this section, the ordinary differential equations (referred to as modal equations of motion), including the nonlinear terms for the amplitudes of dominant components will be derived. Here, the natural frequency of the structure system (expressed by Eq. (9)) is defined by $p_0 = \sqrt{k/(v + d_1 h_1 + d_2 h_2)}$. Namely, p_0 represents the natural frequency of the system where the liquid is assumed to be frozen. The response of the nonlinear-coupled system in the vicinity of $p_0 \cong \omega$ is investigated in the presence of the condition of internal resonance $p_0 \cong 2p_1 \cong 2\bar{p}_1$ among the natural frequencies p_0, p_1 and $\bar{p}_1$. Here, p_1 and $\bar{p}_1$ are defined in Eq. (6) and represent the natural frequencies of the first mode of liquid sloshing in tanks 1 and 2, respectively.

The forced solutions are assumed to be expressed in terms of the eigenfunctions obtained from the corresponding linear analysis according to Galerkin's method:

$$\begin{aligned}\phi_1(x_1, z_1, t) = a_0 + \sum_{n=1}^{\infty}\big[&a_{2n-1}\,\sin(\lambda_{2n-1}x_1)\cosh\{\lambda_{2n-1}(z_1 + h_1)\}/\cosh(\lambda_{2n-1}h_1) \\ &+ a_{2n}\cos(\lambda_{2n}x_1)\cosh\{\lambda_{2n}(z_1 + h_1)\}/\cosh(\lambda_{2n}h_1)\big],\end{aligned} \tag{14a}$$

$$\eta_1(x_1, t) = \sum_{n=1}^{\infty}[b_{2n-1}\,\sin(\lambda_{2n-1}x_1) + b_{2n}\cos(\lambda_{2n}x_1)], \tag{14b}$$

$$\begin{aligned}\phi_2(x_2, z_2, t) = \bar{a}_0 + \sum_{n=1}^{\infty}\big[&\bar{a}_{2n-1}\,\sin(\lambda_{2n-1}x_2)\cosh\{\lambda_{2n-1}(z_2 + h_2)\}/\cosh(\lambda_{2n-1}h_2) \\ &+ \bar{a}_{2n}\cos(\lambda_{2n}x_2)\cosh\{\lambda_{2n}(z_2 + h_2)\}/\cosh(\lambda_{2n}h_2)\big],\end{aligned} \tag{14c}$$

$$\eta_2(x_2, t) = \sum_{n=1}^{\infty}\big[\bar{b}_{2n-1}\,\sin(\lambda_{2n-1}x_2) + \bar{b}_{2n}\cos(\lambda_{2n}x_2)\big], \tag{14d}$$

where a_0, $\bar{a}_0$, a_n, $\bar{a}_n$, b_n and $\bar{b}_n$ are the functions of time. Here, we introduce a small parameter ε and then assume the unknown variables and other system parameters to have the following orders in the same way as that in the previous paper [29]:

$$\begin{aligned}&a_1, \bar{a}_1, b_1, \bar{b}_1, z_0; c, \zeta_n, \bar{\zeta}_n = O(\varepsilon^{1/3}), \\ &a_0, \bar{a}_0, a_2, \bar{a}_2, a_3, \bar{a}_3, b_2, \bar{b}_2, b_3, \bar{b}_3 = O(\varepsilon^{2/3}), \\ &a_n, \bar{a}_n, b_n, \bar{b}_n < O(\varepsilon^{3/3}) \ \text{ for } \ n \geqslant 4, \ \ F_0 = O(\varepsilon^{3/3}).\end{aligned} \tag{15}$$

The ordering technique similar to Eq. (15) was also adapted in Refs. [12,14,32]. In Ref. [14], the third modes of sloshing (corresponding to the amplitudes $a_3, \bar{a}_3, b_3$ and $\bar{b}_3$) were assumed to $O(\varepsilon)$. It was stated that the condition $h/l \geqslant 0.28$ was required for calculation in Ref. [14]. However, it should be noted that $b_1 = O(\varepsilon^{1/3})$ and $b_2 = b_3 = O(\varepsilon^{2/3})$ are assumed in order to consider the effect of the third sloshing mode in the same order as the second mode.

Substituting Eq. (14) into Eq. (8), we obtain the equation for the pressure P_i. Then, substituting that equation for P_i into Eq. (10), and integrating the resulting equation mathematically, one can obtain the fluid forces F_i within an accuracy of $O(\varepsilon)$. Consequently, Eq. (9) can be rewritten as follows:

$$Q_1\ddot{z}_0 + c\dot{z}_0 + kz_0 + H_1(\ddot{z}_0, \dot{b}_1, \dot{\bar{b}}_1, b_1, \bar{b}_1) = F_0 \cos \omega t, \tag{16a}$$

where $Q_1 = v + d_1h_1 + d_2h_2$. Q_1 has a physical meaning, the nondimensional mass corresponding to the total mass $M = m + m_1 + m_2$, and it always equals a unit. H_1 represents a nonlinear term (see Appendix A), where a_0, $\bar{a}_0$, a_n and $\bar{a}_n$ have been eliminated by using equations given in Appendix B.

Secondly, substituting Eq. (14) into Eqs. (12) and (13), one equates the constant terms and the coefficients of $\sin(\lambda_n x_i)$ and $\cos(\lambda_n x_i)$ ($n = 1, 2, 3$; $i = 1, 2$) on both sides of these equations within an accuracy of $O(\varepsilon)$, in the same way as that in the previous paper [29]. Then, one can obtain the ordinary differential equations for a_0, $\bar{a}_0$, a_n, b_n, $\bar{a}_n$ and $\bar{b}_n$ (see Appendix B). Consequently, one can obtain the modal equations of motion for tanks 1 and 2 as follows:

$$\text{For tank 1}: \quad \begin{aligned} &\ddot{b}_1 + 2\zeta_1\dot{b}_1 + (1 + \psi_1\ddot{z}_0)b_1 + H_2(\dot{b}_i, b_i) = 0, \\ &\ddot{b}_2 + 2\zeta_2\omega_2\dot{b}_2 + \omega_2^2(1 + \psi_1\ddot{z}_0)b_2 + H_3(\ddot{z}_0, \dot{b}_i, b_i) = 0, \\ &\ddot{b}_3 + 2\zeta_3\omega_3\dot{b}_3 + \omega_3^2(1 + \psi_1\ddot{z}_0)b_3 + H_4(\dot{b}_i, b_i) = 0, \end{aligned} \tag{16b}$$

$$\text{For tank 2}: \quad \begin{aligned} &\ddot{\bar{b}}_1 + 2\bar{\zeta}_1\bar{\omega}_1\dot{\bar{b}}_1 + \bar{\omega}_1^2(1 + \bar{\psi}_1\ddot{z}_0)\bar{b}_1 + H_5(\dot{\bar{b}}_i, \bar{b}_i) = 0, \\ &\ddot{\bar{b}}_2 + 2\bar{\zeta}_2\bar{\omega}_2\dot{\bar{b}}_2 + \bar{\omega}_2^2(1 + \bar{\psi}_1\ddot{z}_0)\bar{b}_2 + H_6(\ddot{z}_0, \dot{\bar{b}}_i, \bar{b}_i) = 0, \\ &\ddot{\bar{b}}_3 + 2\bar{\zeta}_3\bar{\omega}_3\dot{\bar{b}}_3 + \bar{\omega}_3^2(1 + \bar{\psi}_1\ddot{z}_0)\bar{b}_3 + H_7(\dot{\bar{b}}_i, \bar{b}_i) = 0, \end{aligned} \tag{16c}$$

where ${\omega_n}^2 = \psi_n/\psi_1$ and $\bar{\omega}_n^2 = \bar{\psi}_n/\psi_1$ [$\psi_n = \lambda_n \tanh(\lambda_n h_1)$ and $\bar{\psi}_n = \lambda_n \tanh(\lambda_n h_2)$], which represent dimensionless natural frequencies of the nth sloshing mode in tanks 1 and 2, respectively. H_j ($j = 2, 3, \ldots, 7$) represent nonlinear terms (also see Appendix A). In Eqs. (16a)–(16c), a_0, $\bar{a}_0$, a_n and $\bar{a}_n$ have been eliminated. The viscous damping terms such as $2\zeta_n\omega_n\dot{b}_n$ are added into Eqs. (16b) and (16c) considering the effect of damping for sloshing motion. Here, ζ_n represents the damping ratio corresponding to the nth sloshing mode. Eq. (16b) is the same as the equation, which has been obtained in the Ref. [29]. Eq. (16) enables one to obtain time histories for the structure/fluid interaction system by carrying out a numerical simulation.

2.3. Frequency response curves near the tuning frequency

An FFT analysis generally gives the information about the frequency components that are predominantly involved in the time histories. Van der Pol's method [31] is used together with the FFT results to determine the resonance curves for the system. Based on the FFT results for the numerical simulation of Eq. (16) near the resonant frequency $\omega \cong p_0 \cong 2p_1 \cong 2\bar{p}_1$, one can assume the solutions of the forced oscillation:

$$\begin{aligned} z_0 &= u_1 \cos \omega t - v_1 \sin \omega t, \\ b_1 &= u_2 \cos \tfrac{1}{2}\omega t - v_2 \sin \tfrac{1}{2}\omega t + e_1 \cos \tfrac{3}{2}\omega t - f_1 \sin \tfrac{3}{2}\omega t, \\ b_2 &= e_2 \cos \omega t - f_2 \sin \omega t + r_2, \\ b_3 &= e_3 \cos \tfrac{1}{2}\omega t - f_3 \sin \tfrac{1}{2}\omega t + e_4 \cos \tfrac{3}{2}\omega t - f_4 \sin \tfrac{3}{2}\omega t, \\ \bar{b}_1 &= \bar{u}_2 \cos \tfrac{1}{2}\omega t - \bar{v}_2 \sin \tfrac{1}{2}\omega t + \bar{e}_1 \cos \tfrac{3}{2}\omega t - \bar{f}_1 \sin \tfrac{3}{2}\omega t, \\ \bar{b}_2 &= \bar{e}_2 \cos \omega t - \bar{f}_2 \sin \omega t + \bar{r}_2, \\ \bar{b}_3 &= \bar{e}_3 \cos \tfrac{1}{2}\omega t - \bar{f}_3 \sin \tfrac{1}{2}\omega t + \bar{e}_4 \cos \tfrac{3}{2}\omega t - \bar{f}_4 \sin \tfrac{3}{2}\omega t, \end{aligned} \tag{17}$$

where the amplitudes ($u_i, v_i, \bar{u}_2, \bar{v}_2, e_j, f_j, \bar{e}_j$ and $\bar{f}_j$) and the constant terms (r_2 and $\bar{r}_2$) are the unknown functions varying slowly with time. Here, $i = 1$ and 2; $j = 1, 2, 3$ and 4. Their magnitudes are assumed to follow Eq. (11) and be decreased by $O(\varepsilon^{2/3})$ during every differentiation of them with respect to time in the same manner as our previous paper [16]. Namely,

$$u_i, v_i, \bar{u}_2, \bar{v}_2 \approx O(\varepsilon^{1/3}), \quad e_j, f_j, r_2, \bar{e}_j, \bar{f}_j, \bar{r}_2 \approx O(\varepsilon^{2/3}),$$

$$\dot{u}_i, \dot{v}_i, \dot{\bar{u}}_2, \dot{\bar{v}}_2 \approx O(\varepsilon^{3/3}), \quad \dot{e}_j, \dot{f}_j, \dot{r}_2, \dot{\bar{e}}_j, \dot{\bar{f}}_j, \dot{\bar{r}}_2 \approx O(\varepsilon^{4/3}),$$
$$\ddot{u}_i, \ddot{v}_i, \ddot{\bar{u}}_2, \ddot{\bar{v}}_2 \approx O(\varepsilon^{5/3}), \quad \ddot{e}_j, \ddot{f}_j, \ddot{r}_2, \ddot{\bar{e}}_j, \ddot{\bar{f}}_j, \ddot{\bar{r}}_2 \approx O(\varepsilon^{2}). \tag{18}$$

As for the system with a single tank in Ref. [29], the time histories are calculated at $\omega = 2.03$ in Fig. 2 where sloshing occurs in comparative large amplitude and higher-order sloshing modes appear. It has already been examined in Ref. [29] that any other frequency components did not appear significantly except for the frequency components considered in Eq. (17). Substituting Eq. (17) into Eq. (16) and taking a harmonic balance for the frequencies ω, $(1/2)\omega$ and $(3/2)\omega$, and the constant terms under the order estimation (18), respectively, one can obtain the ordinary differential equations and the algebraic equations for those unknown variables as follows:

$$\begin{aligned}
\dot{u}_1 &= G_1(u_i, v_i, \bar{u}_2, \bar{v}_2, e_1, f_1, \bar{e}_1, \bar{f}_1),\\
\dot{v}_1 &= G_2(u_i, v_i, \bar{u}_2, \bar{v}_2, e_1, f_1, \bar{e}_1, \bar{f}_1),\\
\dot{u}_2 &= G_3(u_i, v_i, e_i, f_i, r_2),\\
\dot{v}_2 &= G_4(u_i, v_i, e_i, f_i, r_2),\\
\dot{\bar{u}}_2 &= G_5(u_1, v_1, \bar{u}_2, \bar{v}_2, \bar{e}_i, \bar{f}_i, \bar{r}_2),\\
\dot{\bar{v}}_2 &= G_6(u_1, v_1, \bar{u}_2, \bar{v}_2, \bar{e}_i, \bar{f}_i, \bar{r}_2).\\
G_m(u_i, v_i, e_j, f_j, r_2) &= 0,\\
G_n(u_1, v_1, \bar{u}_2, \bar{v}_2, \bar{e}_j, \bar{f}_j, \bar{r}_2) &= 0.
\end{aligned} \tag{19}$$

Functions G_l ($l = 1, 2, \ldots, 6$), G_m ($m = 7, 8, \ldots, 15$) and G_n ($n = 16, 17, \ldots, 24$) in Eq. (19) represent the nonlinear terms which consist of the variables in their parentheses (where $i = 1, 2$ and $j = 1, 2, 3, 4$). For example, u_i in function G_1 implies that it includes u_1 and u_2. The complete forms of Eq. (19) are omitted here. One can calculate the steady-state solutions and their stabilities from Eq. (19) in the same manner as our previous paper [29].

An sdof system, by replacing the liquid in the tank to a same mass of solid body, is used to compare with the nonlinear-coupled partially filled liquid system. The response for the sdof system is given by

$$z_0 = A\cos(\omega t + \beta), \tag{20a}$$

where

$$A = \frac{F_0}{\sqrt{\{k - Q_1\omega^2\} + (c\omega)^2}}, \quad \beta = -\tan^{-1}\left[\frac{c\omega}{k - Q_1\omega^2}\right]. \tag{20b}$$

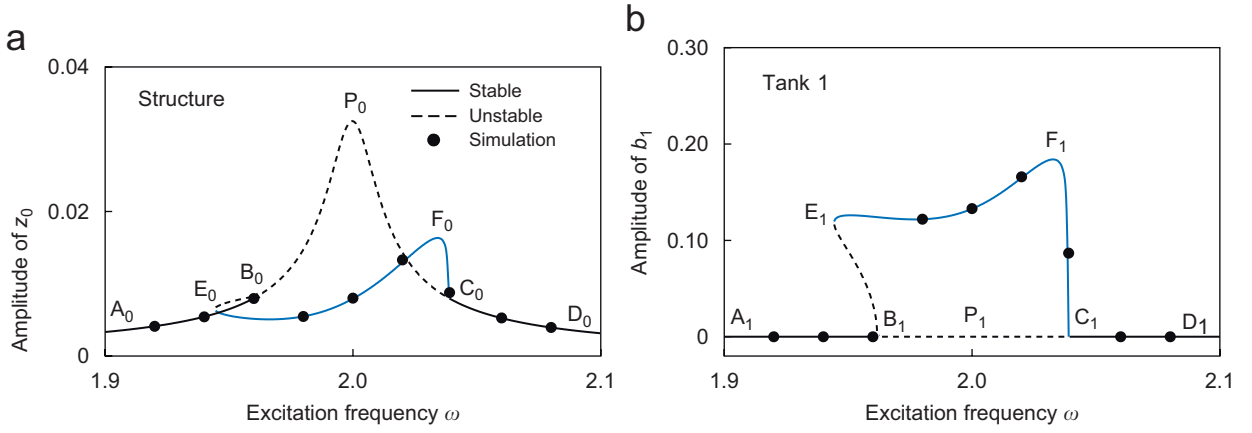

Fig. 2. Theoretical resonance curves for a single-tank system when $v = 0.93$, $k = 4.0$, $c = 0.02$, $h_1 = 0.60$, $h_2 = 0$, $d_1 = 0.117$, $d_2 = 0$, $\zeta_n = 0.015$ and $F_0 = 0.0013$: (a) the amplitude of the ω component of z_0; (b) the amplitude of the $(1/2)\omega$ component of b_1.

3. Numerical results

In numerical calculation, we will choose the values of parameters in such way that the relationship $p_0 \cong 2p_1 \cong 2\bar{p}_1$ holds among the natural frequencies of the structure and sloshing in tanks 1 and 2.

Fig. 2 shows the theoretical frequency response curves for the frequency component ω of the structure's displacement z_0 (with an amplitude $\sqrt{u_1^2+v_1^2}$) and for the frequency component $(1/2)\omega$ of the sloshing elevation b_1 (with an amplitude $\sqrt{u_2^2+v_2^2}$) when only one rectangular tank is used. The values of parameters are $\nu = 0.93$, $k = 4.0$, $c = 0.02$, $h_1 = 0.60$, $h_2 = 0$, $d_1 = 0.117$, $d_2 = 0$, $\zeta_n = 0.015$ and $F_0 = 0.0013$. The values of the damping ratios ζ_n and excitation amplitude F_0 are based on the experimental data to be discussed later. The solid and broken lines represent the stable and unstable steady-state solutions, respectively. The symbol '●' represents the corresponding amplitude obtained by numerical simulation and the FFT analysis. The Adams method is applied to Eqs. (16a)–(16c) in numerical simulation. The steady state solution calculated from Eq. (19) in Section 2.3 is given to the initial condition for the numerical simulation. Fig. 2 is identical to the response curves shown in the previous paper [29], but this figure will be compared with the frequency response curves for using two liquid-filled tanks. The curve $A_0B_0P_0C_0D_0$ in Fig. 2(a) is the same as that for the sdof system, given by Eq. (20b), except for the stability of the steady-stale solution. When the sloshing is generated in the tank, the curve $B_0P_0C_0$ becomes unstable as well as the corresponding curve $B_1P_1C_1$ in Fig. (2b). In addition, finite amplitude curves $E_0F_0C_0$ and $E_1F_1C_1$ appear due to the effect of the nonlinear fluid force.

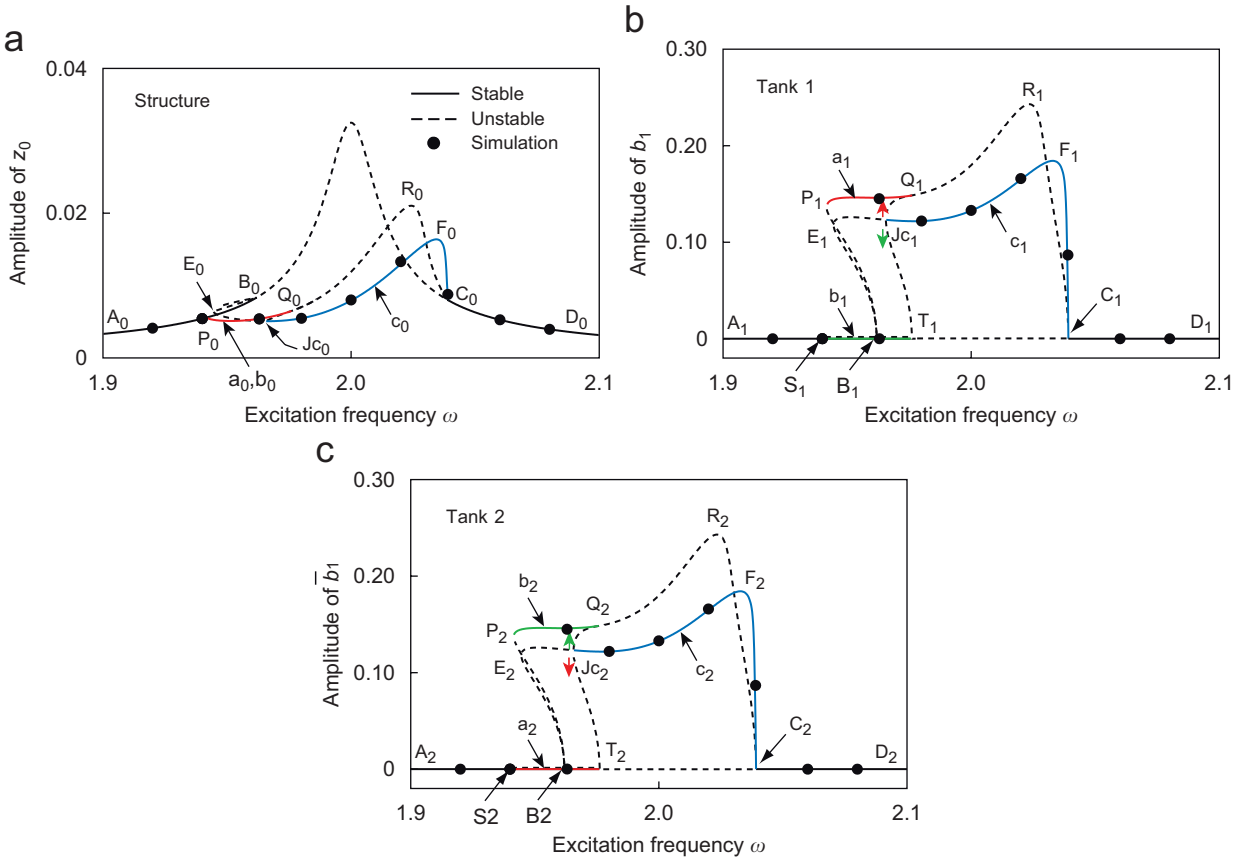

Fig. 3. Theoretical frequency response curves for a two-tank system when $\nu = 0.93$, $k = 4.0$, $c = 0.02$, $h_1 = h_2 = 0.60$, $d_1 = d_2 = 0.0583$, $\zeta_n = 0.015$ and $F_0 = 0.0013$: (a) the amplitude of the ω component of z_0; (b) the amplitude of the $(1/2)\omega$ component of b_1; (c) the amplitude of the $(1/2)\omega$ component of $\bar{b}_1$.

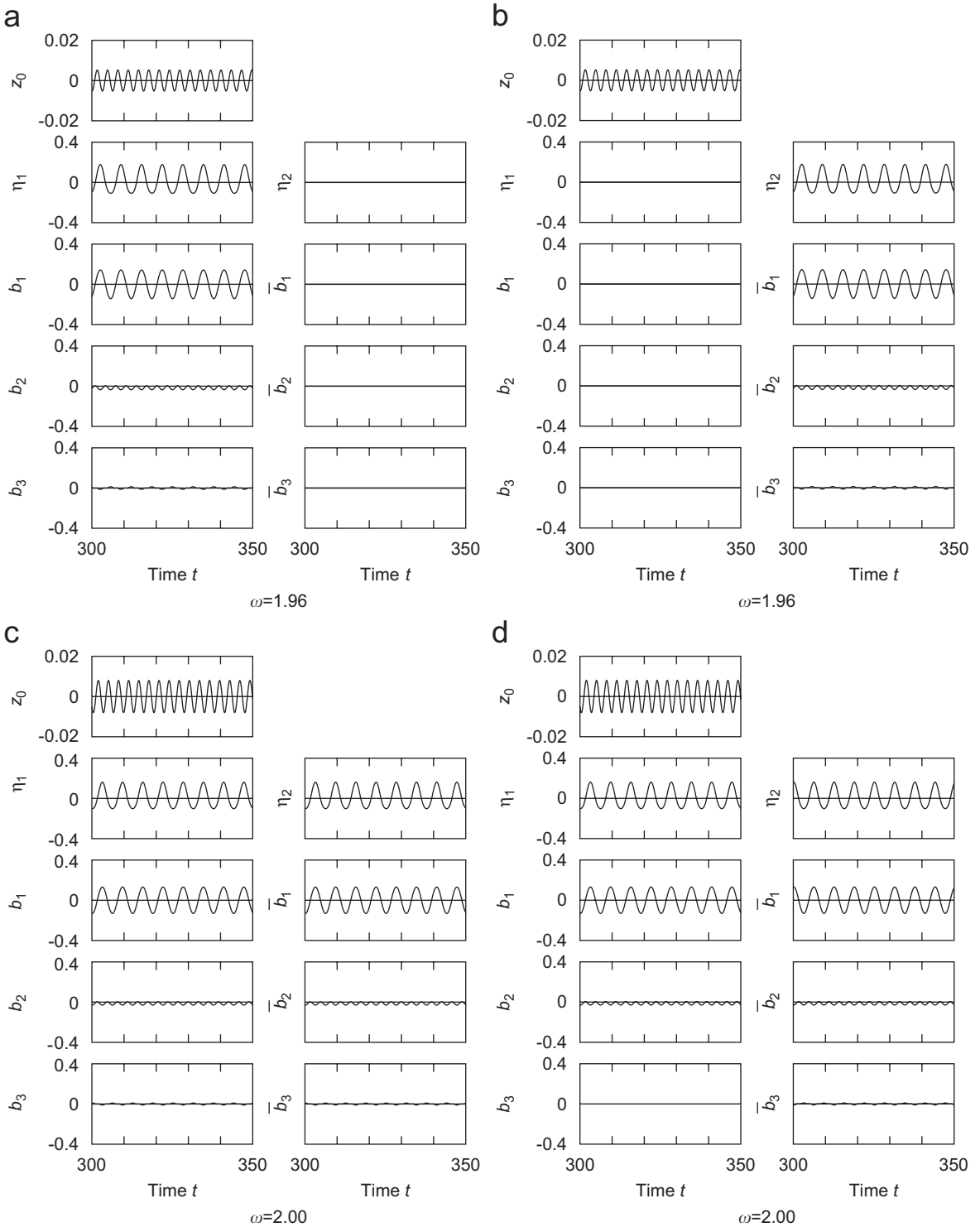

Fig. 4. Stationary time histories at $x_1 = x_2 = 0.5$ in Fig. 3: (a) $\omega = 1.96$; (b) $\omega = 1.96$; (c) $\omega = 2.00$; (d) $\omega = 2.00$.

It should be noted that the natural frequencies of the three-dimensional waves are all larger than double the lowest natural frequency p_1 of the two-dimensional wave when the values of the system parameters in Fig. 2 are given. Therefore, three-dimensional waves never occur for the system parameters discussed hereinafter (see Appendix C).

3.1. Influence of liquid levels

In this section, the frequency response curves will be shown to demonstrate the influence due to the change of liquid levels when two tanks are used.

Figs. 3(a)–(c) show the frequency response curves for the structure, the sloshing elevations b_1 in tank 1 and $\bar{b}_1$ in tank 2 (with an amplitude $\sqrt{\bar{u}_2^2+\bar{v}_2^2}$), respectively, when $\nu=0.93$, $c=0.02$, $k=4.0$, $h_1=h_2=0.60$, $d_1=d_2=0.0583$, $\zeta_n=\bar{\zeta}_n=0.015$ and $F_0=0.0013$. The only difference between the systems in Figs. 2 and 3 exist in that a single tank with a width 0.117 (i.e., $d_1=0.117$ and $d_2=0$) in Fig. 2 is divided into two tanks with a half-width 0.0583 (i.e., $d_1=d_2=0.0583$) in Fig. 3. The theoretical resonance curves agree well with the results of numerical simulation. The curves $E_1J_{c1}F_1C_1$ and $E_2J_{c2}F_2C_2$ correspond to the curve $E_1F_1C_1$ in Fig. 2(b) and they have the identical amplitude, but the parts E_1J_{c1} and E_2J_{c2} are unstable in Fig. 3. The ranges B_1C_1 and B_2C_2 of the excitation frequency coincide with the range B_1C_1 in Fig. 2. In addition, new branches $B_1P_1Q_1R_1C_1$ and $T_1J_{c1}Q_1$ in Fig. 3(b) and $B_2P_2Q_2R_2C_2$ and $T_2J_{c2}Q_2$ in Fig. 3(c) appear. It should be noted that the curves E_1J_{c1} and E_1J_{c1} are unstable although a part of the corresponding curve is stable for the single-tank system in Fig. 2(b). While the excitation frequency ω is decreasing from 2.1 in Fig. 3, sloshing starts to appear simultaneously near $\omega=2.05$ in both the tanks and then it occurs along the branches 'c_1' ($J_{c1}F_1C_1$) and

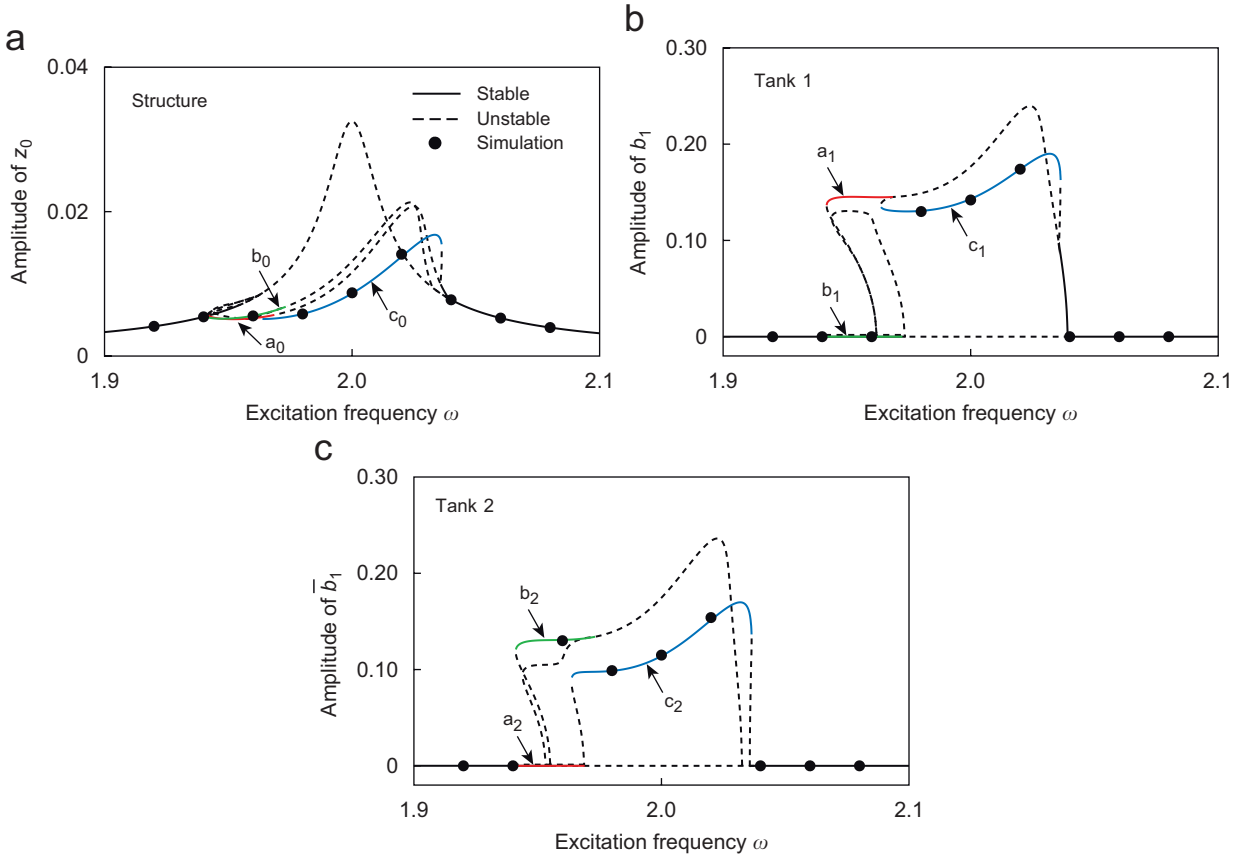

Fig. 5. Same as Fig. 3, but $h_1=0.60$, $h_2=0.55$ and $d_1=d_2=0.0609$: (a) the amplitude of the ω component of z_0; (b) the amplitude of the $(1/2)\omega$ component of b_1; (c) the amplitude of the $(1/2)\omega$ component of $\bar{b}_1$.

'c_2' ($J_{c2}F_2C_2$) in Figs. 3(b) and (c), respectively. The branch 'c_0' ($J_{c0}F_0C_0$) in Fig. 3(a) appears corresponding to these branches. This type of response is termed the 'double-mode' solution. As ω continues to decrease, the amplitude of sloshing in tank 1 jumps from the branch 'c_1' to the branch 'a_1' (P_1Q_1) at point J_{c1}. At the same time, the amplitude of sloshing in tank 2 jumps at point J_{c2} from the branch 'c_2' to the branch 'a_2' ($S_2B_2T_2$) with zero amplitude, namely the liquid surface in tank 2 remains stationary. Therefore, sloshing can appear only in tank 1 and this type of response is termed the 'single-mode' solution. It should be noted that the amplitude of the single-mode solution 'a_1' is larger than that of the branch $E_1F_1C_1$ in Fig. 2, although the amplitude of the double-mode solution 'c_1' or 'c_2' is exactly alike. Depending on the infinitesimal disturbance at points J_{c1} and J_{c2}, the amplitude of sloshing may jump to the branch 'b_1' ($S_1B_1T_1$) with zero amplitude in tank 1, and at the same time it jumps to the branch 'b_2' (P_2Q_2) in tank 2. Consequently, the single-mode solution occurs either in tank 1 or in tank 2. This phenomenon is similar to the mode localization in nonlinear systems [33], that sometimes occurs in the multidegree-of-freedom system coupled by a weak nonlinear stiffness. Similarly, the first equation (for b_1) in Eq. (16b) is indirectly coupled with the first equation (for $\bar{b}_1$) in Eq. (16c) by means of the nonlinear terms including $\ddot{z}_0$. These single-mode and double-mode solutions can also occur in a two-degree-of-freedom autoparametric vibration absorber with multiple pendulums [34]. The linear analysis can merely describe that the interval B_1C_1 or B_2C_2 is an unstable excitation frequency region generated by the parametric excitation. However, the nonlinear analysis gives the new information as mentioned above.

Fig. 4 shows the stationary time histories obtained by numerically integrating Eq. (16). The steady-state solutions obtained in Fig. 3 are used for the initial values for z_0, b_1 and $\bar{b}_1$ in the simulation. The time histories are observed at $x_1 = x_2 = 0.5$. Figs. 4(a) and (b) are the time histories corresponding to the single-mode

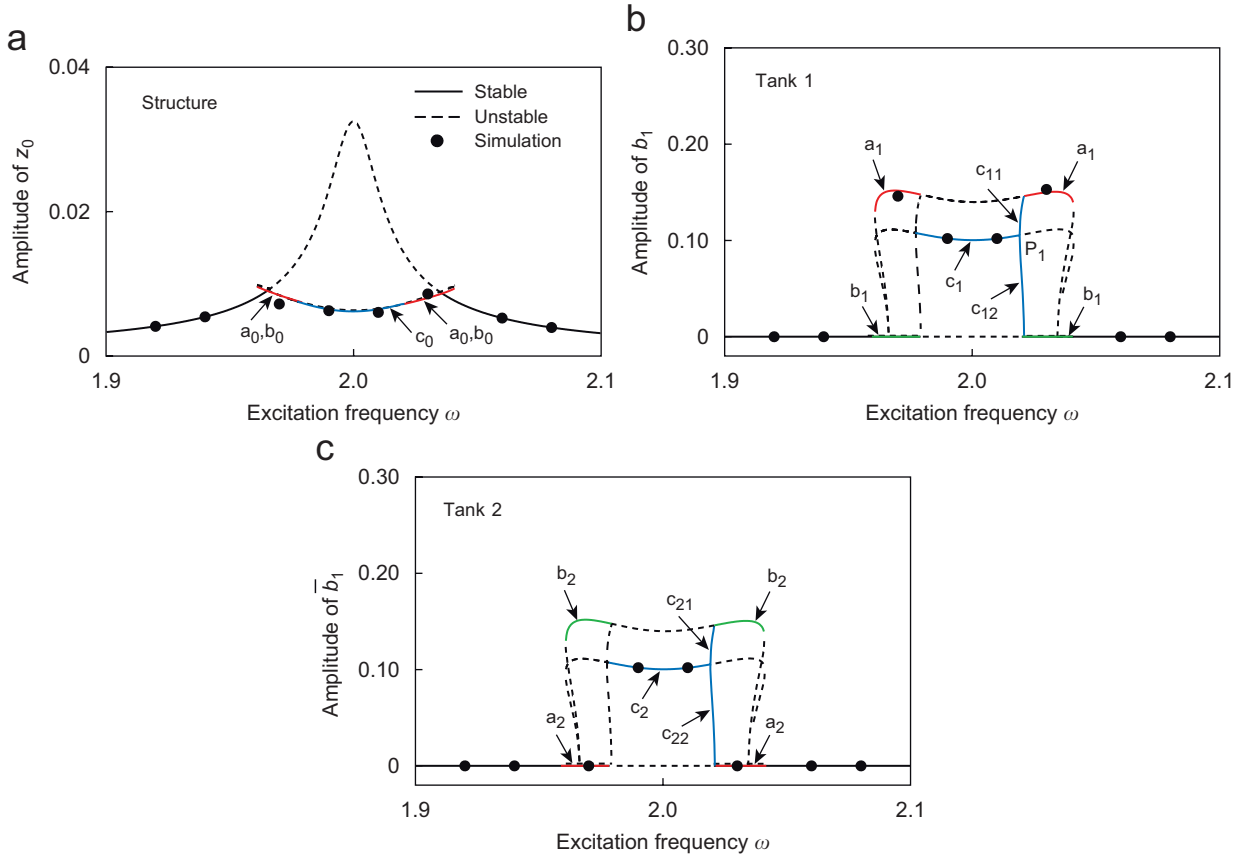

Fig. 6. Same as Fig. 3, but $h_1 = h_2 = 0.343$ and $d_1 = d_2 = 0.102$: (a) the amplitude of the ω component of z_0; (b) the amplitude of the $(1/2)\omega$ component of b_1; (c) the amplitude of the $(1/2)\omega$ component of $\bar{b}_1$.

solution when $\omega = 1.96$. Figs. 4(c) and (d) are the time histories corresponding to the double-mode solution when $\omega = 2.00$. The elevations η_1 and η_2 of the liquid surfaces are in phase in Fig. 4(c), but they are anti-phase in Fig. 4(d).

Fig. 5 shows the frequency response curves in the case where the value of h_2 is decreased from 0.6 in Fig. 3 to 0.55. Here $d_1 = d_2 = 0.0609$, because $Q_1(= v + d_1h_1 + d_2h_2)$ must be equal to one. The left boundary points of the double-mode solutions 'c_1' and 'c_2' change saddle-node bifurcation points from pitchfork bifurcation ones. It can be seen from Fig. 5 that the single-mode solution corresponding to the branch 'a_1' or 'b_2' appear in different amplitudes and that the double-mode solutions corresponding to the branches 'c_1' and 'c_2' occur simultaneously. The amplitudes of the single- and double-mode solutions are larger in tank 1 and smaller in tank 2 than those in Fig. 3, because there is some discrepancy in the internal resonance relationship $p_0 = 2p_1 = 2\bar{p}_1$ in Fig. 5.

Fig. 6 shows the frequency response curves, whose parameters are $h_1 = h_2 = 0.343$ and $d_1 = d_2 = 0.102$, changed from Fig. 3. The shape of the response curve for z_0 becomes flat. This implies that the present case can exhibit a high performance as a TLD. This value $h_i = 0.343$ may correspond to the critical liquid level which was examined by Fultz [11] and Waterhouse [15]. The single-mode solutions 'a_1' appear in the left and right sides of the response curve in tank 1, vice versa, the single-mode solutions 'b_2' in tank 2. The double-mode solutions 'c_1' and 'c_2' appear in the middle of the response curves. While the excitation frequency is increasing, the amplitude of the sloshing in tank 1 changes along the branch 'c_1' and bifurcates at point P_1. Then, it changes to the branch 'a_1' via the branch 'c_{11}'. At the same time, the branch 'c_{22}' appears in tank 2, corresponding to the branch 'c_{11}' in tank 1. Alternatively, the amplitude of the sloshing in tank 1 may change from the branch 'c_1' to the branch 'b_1' via the branch 'c_{12}' depending on a small disturbance.

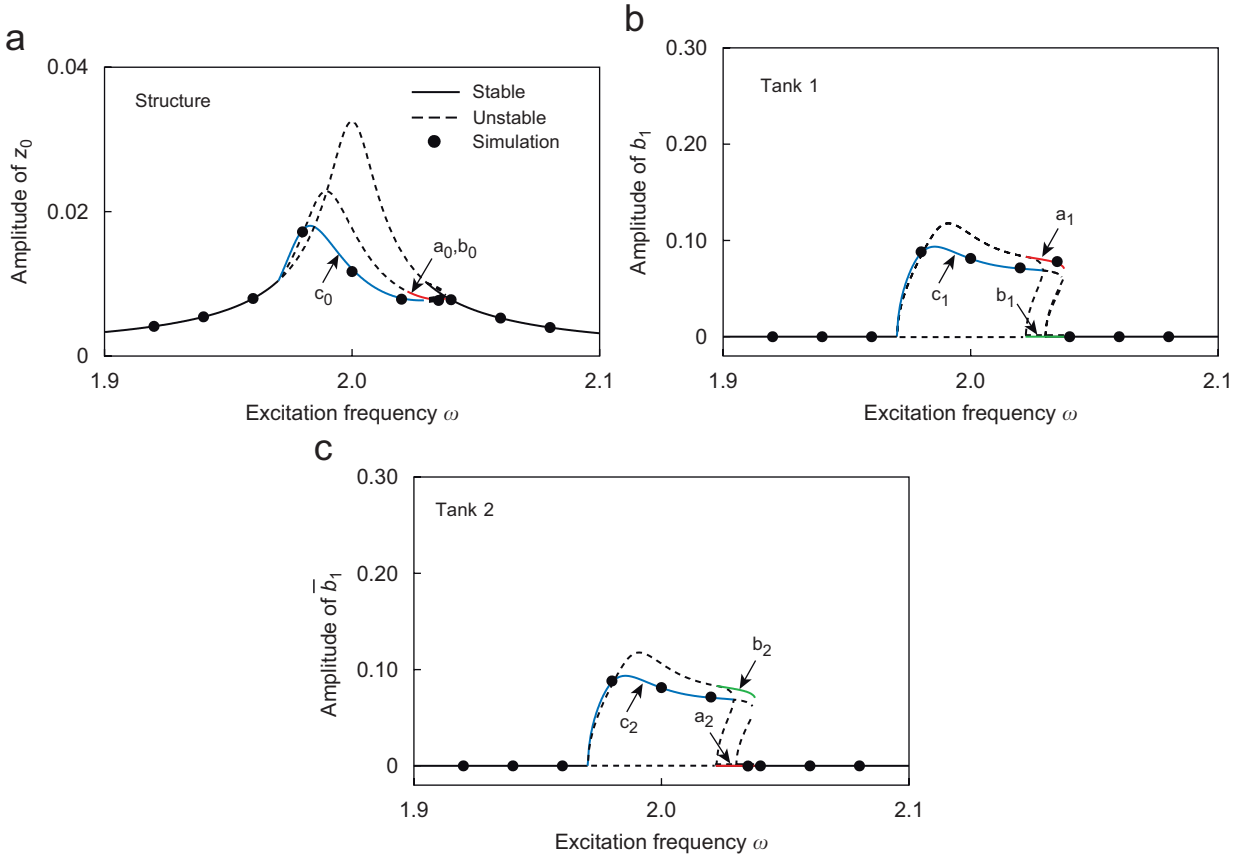

Fig. 7. Same as Fig. 3, but $h_1 = h_2 = 0.25$ and $d_1 = d_2 = 0.140$: (a) the amplitude of the ω component of z_0; (b) the amplitude of the $(1/2)\omega$ component of b_1; (c) the amplitude of the $(1/2)\omega$ component of $\bar{b}_1$.

Fig. 7 shows the frequency response curves for lower liquid levels when the parameters are changed as $h_1 = h_2 = 0.25$ and $d_1 = d_2 = 0.140$ from Fig. 3. The single-mode solutions appear on the right side of the response curves. It should be noted that $h_1 = h_2 = 0.25$ may be most probably away from the validity of the ordering assumption (15).

3.2. Influence of the mistuning

In this section, the influence of the mistuning on the response curves is discussed. The detuning parameters $\sigma_1 = p_0 - 2p_1$ and $\bar{\sigma}_1 = p_0 - 2\bar{p}_1$ are introduced. Fig. 8 shows the frequency response curves when only the value of the spring constant k is changed from $k = 4.0$ in Fig. 5 to $k = 3.78$. In Fig. 8, $\sigma_1 = -0.056$, and $\bar{\sigma}_1 = -0.039$. The double-mode solutions 'c_1' and 'c_2' appear separately. The unstable steady-state solutions appear during the intervals G_1H_1 and G_2H_2 on the branches 'a_1' and 'b_2', respectively, which are the single-mode solutions. The excitation frequency range of the interval G_1H_1 is larger than that of G_2H_2, because h_1 is larger than h_2. It is observed by numerical simulation using Eq. (16) that amplitude-phase-modulated motion (abbreviated by an 'APM' motion) appears at interval G_1H_1 and G_2H_2. Some of their time histories are shown in Fig. 9. Therefore, G_i and H_i $(i = 1, 2)$ are Hopf bifurcation points, as seen in Ref. [29]. The vertical thin lines represent the magnitude of the modulated amplitude. In most cases, this APM motion can appear in the vicinity of the unstable branch G_1H_1 or G_2H_2, because these branches are still the single-mode solutions. Exceptionally, both amplitude of b_1 (corresponding to the branch 'a_1') and amplitude of $\bar{b}_1$ (corresponding to the branch 'a_2') are simultaneously modulated at $\omega = 1.920$.

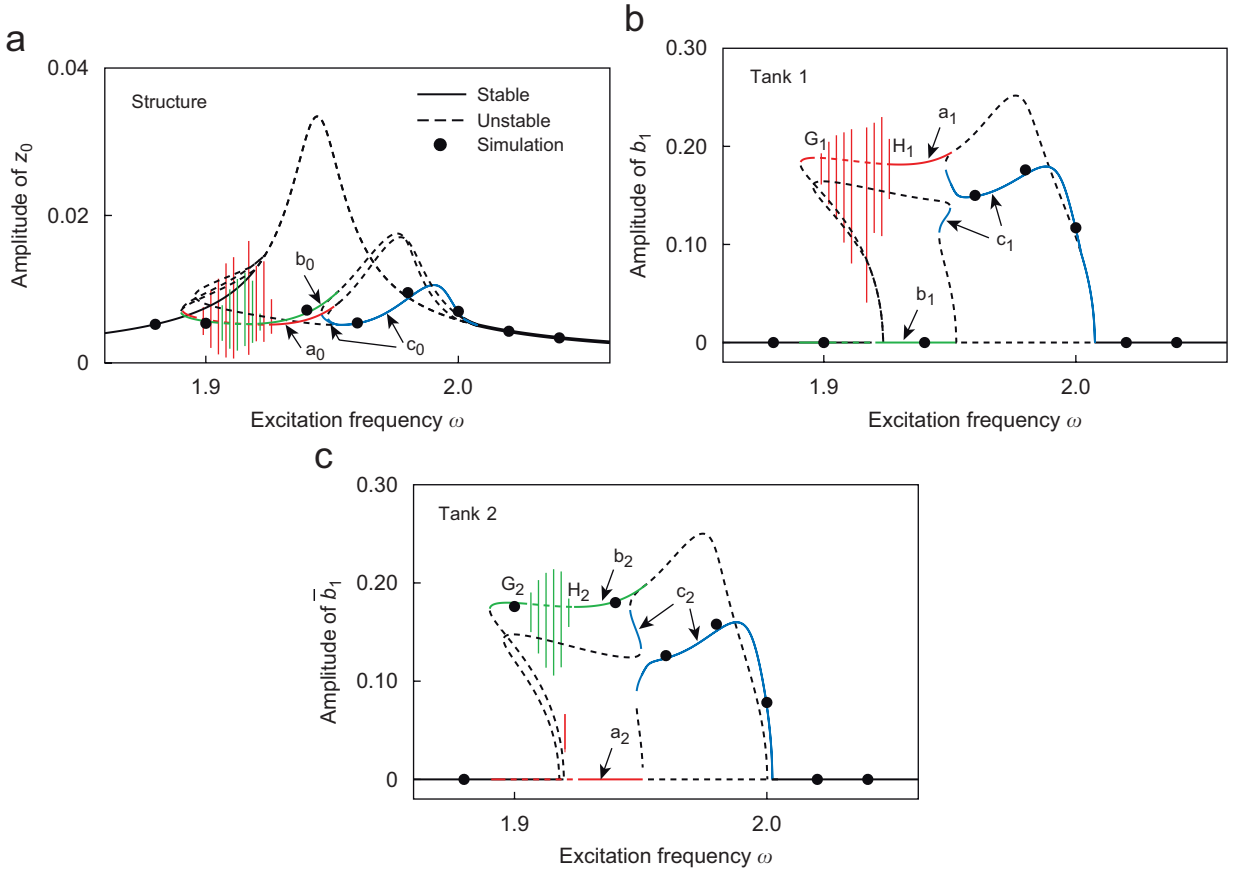

Fig. 8. Same as Fig. 5, but $k = 3.78$ ($\sigma_1 = -0.056$ and $\bar{\sigma}_1 = -0.039$): (a) the amplitude of the ω component of z_0; (b) the amplitude of the $(1/2)\omega$ component of b_1; (c) the amplitude of the $(1/2)\omega$ component of $\bar{b}_1$.

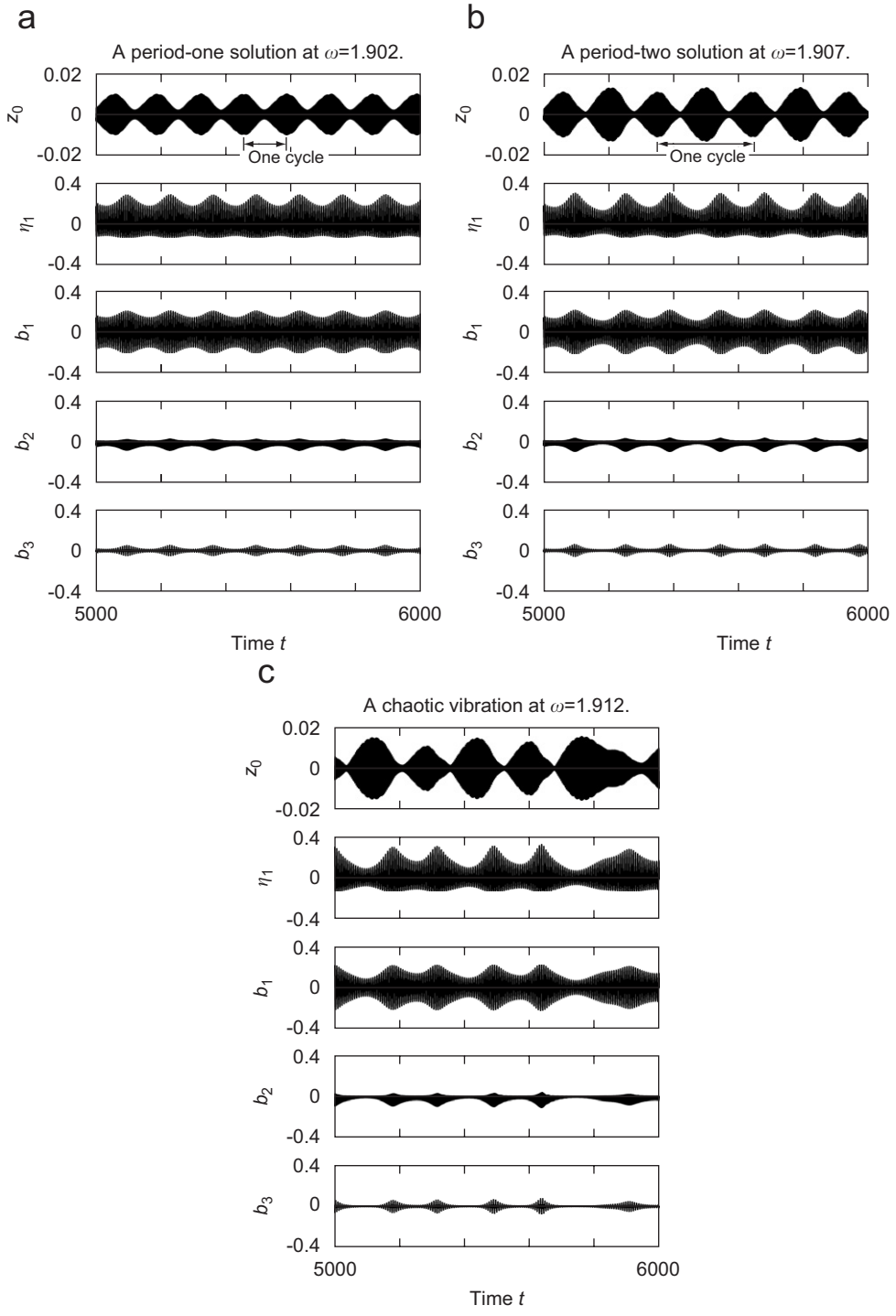

Fig. 9. Stationary time histories at interval G_1H_1 in Fig. 8 when $x_1 = 0.5$: (a) a period-one solution at $\omega = 1.902$; (b) a period-two solution at $\omega = 1.907$; (c) a chaotic vibration at $\omega = 1.912$.

Figs. 9(a)–(c) show the stationary time histories for the APM motion at $\omega = 1.902$, 1.907 and 1.912, respectively. The steady-state solutions corresponding to the branches 'a_1' and 'a_2' are used for the initial values in the numerical simulation. The corresponding time histories for η_2, $\bar{b}_1$, $\bar{b}_2$ and $\bar{b}_3$ are omitted here,

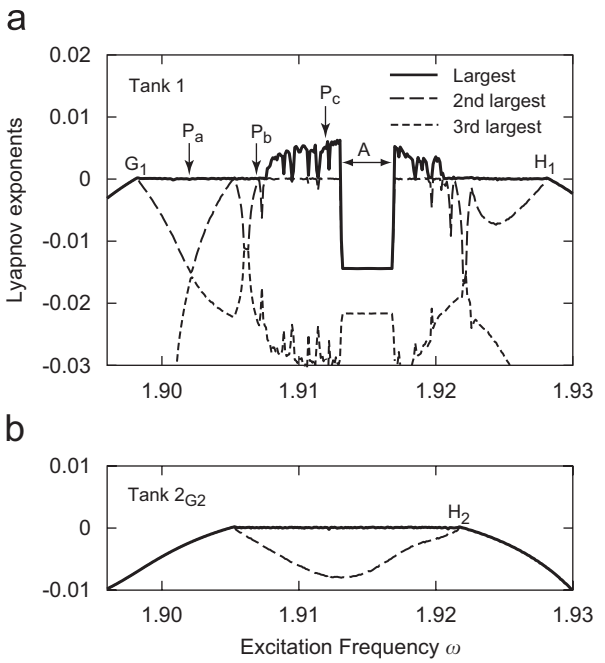

Fig. 10. Lyapunov exponents near the intervals G_1H_1 and G_2H_2 in Fig. 8. Points P_a, P_b and P_c represent the positions of ω corresponding to Figs. 9(a)–(c), respectively. Points G_i and H_i are Hopf bifurcation points.

because their amplitude are infinitesimal. As the excitation frequency increases, amplitude varied once every one cycle of modulation in Fig. 9(a) (which is termed a period-one solution), and twice in Fig. 9(b) (which is termed a period-two solution). The amplitude changes irregularly in Fig. 9(c) and this appears to be a chaotic vibration.

In order to investigate the scenario up to chaotic vibrations in Fig. 9, the Lyapunov exponents are calculated by applying the method of Wolf et al. [35] to Eq. (16). Fig. 10 shows the Lyapunov exponents, including the largest (a full line), the second largest (a broken line) and the third largest ones (a dotted line), versus the excitation frequency ω. Points P_a, P_b and P_c indicate the locations of the excitation frequencies where the time histories are observed in Figs. 9(a)–(c), respectively. Points G_i and H_i ($i = 1, 2$) are Hopf bifurcation points. It is proven from Fig. 10(a) that a chaotic vibration has appeared in Fig. 9(c), because the largest Lyapunov exponent is positive at point P_c. The amplitudes jump to the stable steady-state solutions at the boundaries of the excitation frequency region 'A' in Fig. 10(a). It is also demonstrated from Fig. 10(b) that no chaotic vibrations appear in tank 2.

4. Experimental apparatus

Fig. 11 shows the experimental setup. A T-shaped structure was supported by a coiled spring at the bottom end and it was connected to two 500 mm length arms with ball bearings in their joints in order to keep moving only in the approximately vertical direction (see the front view). Two rectangular liquid-filled tanks 1 and 2 were mounted on the structure. The structure was excited by an electromagnetic exciter (Brüel & Kjær 4808) through a thin aluminum plate. The head of the exciter was controlled by a vibration exciter controller (Brüel & Kjær 1050) in order to keep the amplitude of the head constant regardless of any excitation frequency. A water solution with white watercolors of 0.28% concentration was used as a test liquid so that the light of a laser sensor was able to be reflected on the liquid surface. The vertical displacement z_0^* of the structure was measured by laser sensor S_0. The elevations η_1^* and η_2^* of the water surfaces in tanks 1 and 2 were measured by laser sensors S_1 and S_2 just over the x_i^*-axis, respectively (see the top or side view).

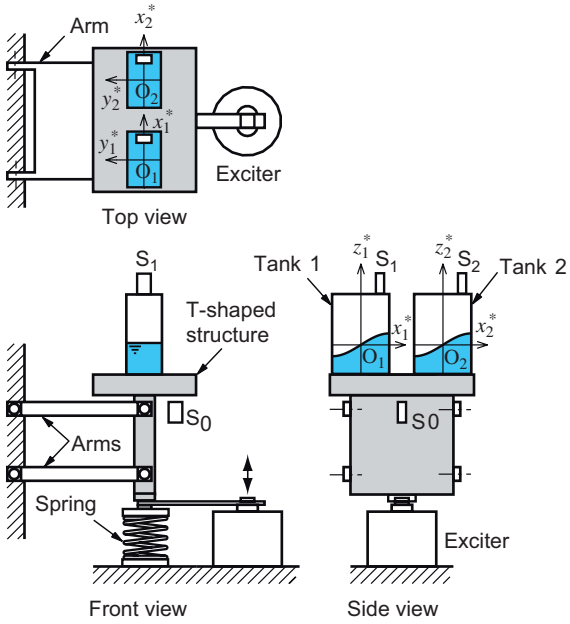

Fig. 11. The setup of the experimental apparatus.

Table 1
Dimensions of apparatuses A–E

Apparatus	A	B	C	D	E
Structure mass: m (kg)	6.687	6.62	6.656	7.203	6.553
Spring constant: k^* (N/m)	8721	8658	8665	8713	4751
Damping coefficient: c^* (Ns/m)	2.64	2.85	2.97	3.14	1.57
Tank length: l^* (mm)	100	100	100	100	120
Width of tank 1: d_1^* (mm)	120	60	60	60	45
Width of tank 2: d_2^* (mm)	—	60	60	60	45
Water depth of tank 1: h_1^* (mm)	60	60	60	60	31
Water depth of tank 2: h_2^* (mm)	—	60	55	55	31
Water mass of tank 1: m_1 (kg)	0.72	0.36	0.36	0.36	0.167
Water mass of tank 2: m_2 (kg)	—	0.36	0.33	0.33	0.167
Damping ratios: ζ_n, $\bar{\zeta}_n$	0.0128	0.0128	0.0128	0.0128	0.019
Force amplitude: F_0^* (N)	0.373	0.46	0.468	0.46	0.334
Natural frequency: p_0 (Hz)	5.461	5.462	5.466	5.288	4.18
Natural frequency (tank 1): p_1 (Hz)	2.729	2.729	2.729	2.729	2.087
Natural frequency (tank 2): $\bar{p}_1$(Hz)	—	2.729	2.706	2.706	2.087
Detuning: σ_1 ($\equiv p_0-2p_1$) Hz	0.003	0.004	0.008	−0.17	0.024
Detuning: $\bar{\sigma}_1$($\equiv p_0-2\bar{p}_1$) Hz	—	0.004	0.054	−0.124	0.024
Position of sensor S_1: x_1^* (mm)	40	40	40	40	40
Position of sensor S_2: x_2^* (mm)	—	40	40	40	40

The dimensions of the experimental apparatuses A–E are listed in Table 1. The internal resonance relationship $p_0 \cong 2p_1 \cong 2\bar{p}_1$ was satisfied in each experimental apparatus. Here, p_0 is given by $1/(2\pi)\sqrt{k/(m+m_1+m_2)}$ Hz, p_1 by $1/(2\pi)\sqrt{g\lambda_1 \tanh(\lambda_1 h_1)}$ Hz and $\bar{p}_1$ by $1/(2\pi)\sqrt{g\lambda_1 \tanh(\lambda_1 h_2)}$ Hz. The value of the damping coefficient c of the structure was identified by curve fitting with the theoretical response curve given by Eq. (20b). The values of the damping ratios ζ_n and $\bar{\zeta}_n$ of the water sloshing were also identified by curve fitting with the theoretical response curves for the nonlinear-coupled system.

5. Experimental results

Figs. 12(a) and (b) show a comparison between the theoretical and experimental resonance curves for the structure and the water surface in apparatus A, carrying a single tank (where the liquid level was high: $h^*/l^* = 0.60$), respectively. It should be noted that these theoretical curves in Figs. 12(a) and (b) represent the

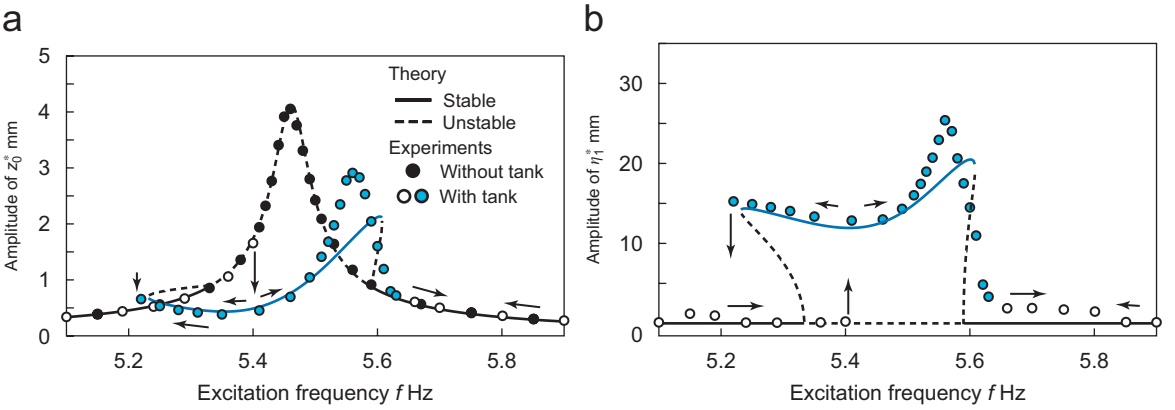

Fig. 12. A comparison between the theoretical and experimental frequency response curves for apparatus A when $h(= h^*/l^*) = 0.6$: (a) amplitudes of z_0^*; (b) amplitudes of η_1^*.

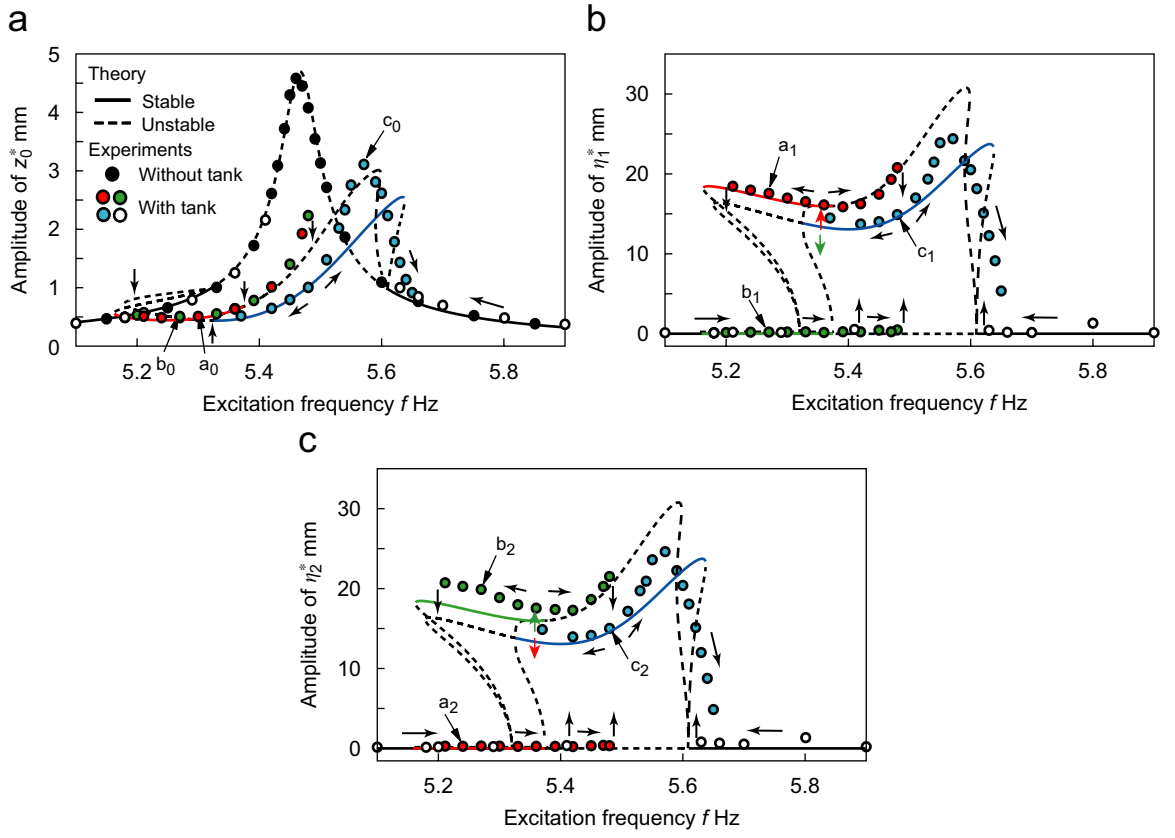

Fig. 13. A comparison between the theoretical and experimental frequency response curves for apparatus B when $h_1^*/l^* = h_2^*/l^* = 0.6$: (a) amplitudes of z_0^*; (b) amplitudes of η_1^*; (c) amplitudes of η_2^*.

amplitudes only for the oscillations of the frequencies ω and $(1/2)\omega$, respectively. The symbol '●' represents the maximum amplitude of an experimental time history in the system where the water was replaced by the solid body of the identical mass. The symbols '○' and '◍' represent the maximum amplitude of time histories in the coupled system carrying the liquid tank. Horizontal or oblique arrows, shown in the figures, represent the direction of changing the excitation frequency. Vertical arrows represent the appearance of jump phenomena in the amplitudes. The theoretical response curves agree well with the experimental data. However, there was some discrepancy between the theoretical and experimental results, because higher-order modes may contribute significantly especially for comparatively large amplitude range of sloshing.

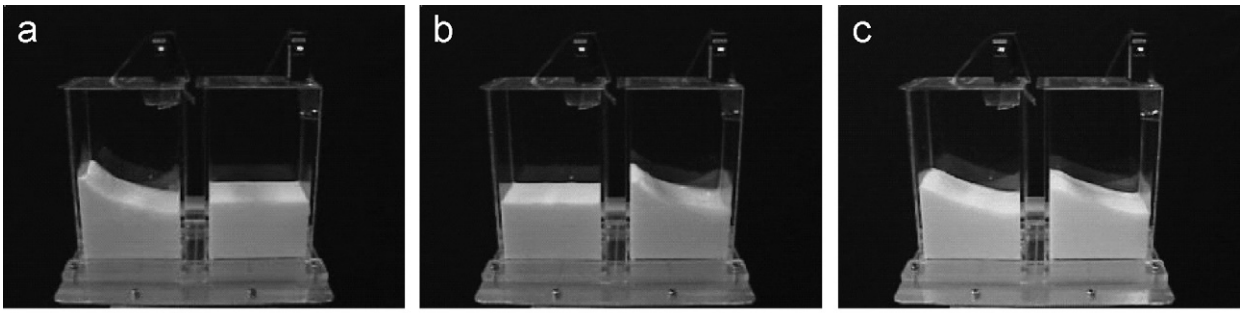

Fig. 14. Photos showing the movement of the liquid surfaces at $f = 5.45$ Hz in Fig. 13: (a) sloshing in tank 1; (b) sloshing in tank 2; (c) sloshing in both tanks.

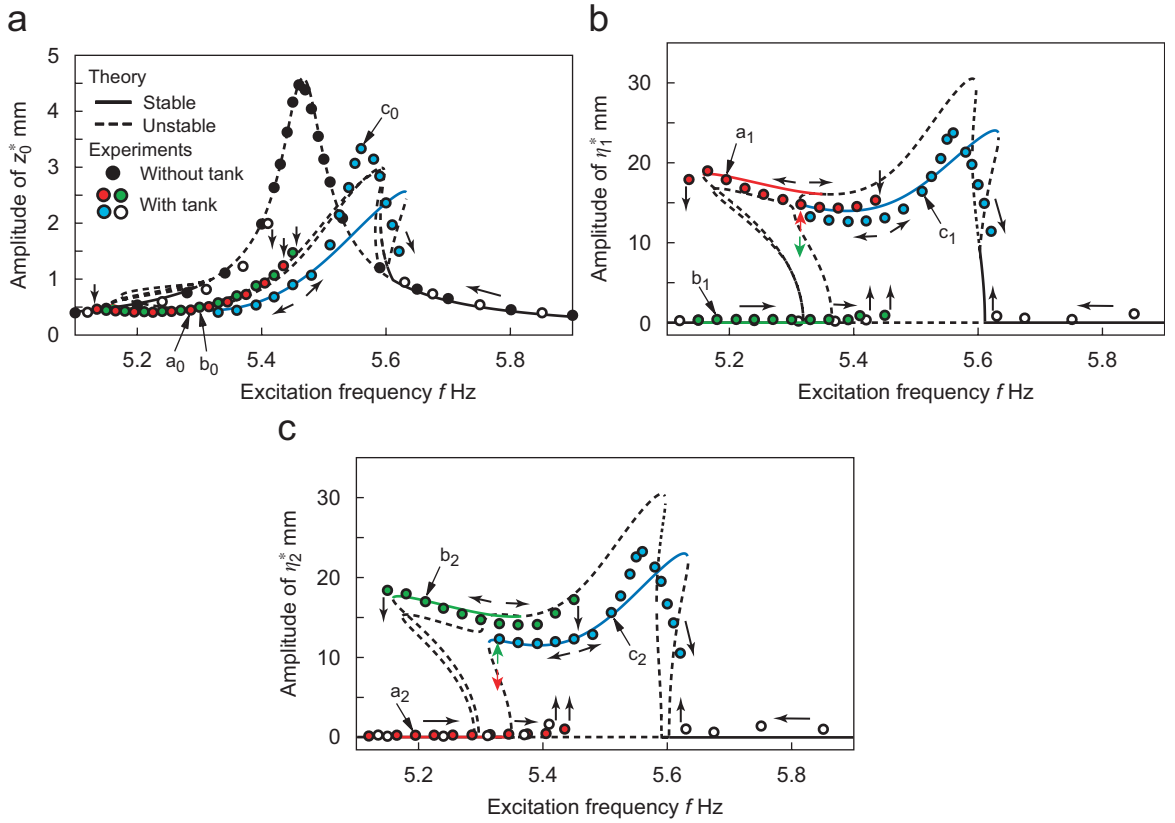

Fig. 15. A comparison between the theoretical and experimental frequency response curves for apparatus C when $h_1^*/l^* = 0.6$ and $h_2^*/l^* = 0.55$: (a) amplitudes of z_0^*; (b) amplitudes of η_1^*; (c) amplitudes of η_2^*.

Fig. 13 shows a comparison between the theoretical and experimental frequency response curves for apparatus B, carrying the two tanks with an identical tank size and an identical liquid level, when $h_1^*/l^* = h_2^*/l^* = 0.60$. The amplitudes of z_0^*, η_1^* and η_2^* are shown in Figs. 13(a)–(c), respectively. The double-mode solutions 'c_1' and 'c_2' appeared, being plotted by the symbol '●'. A pair of the branches 'a_1' and 'a_2' (plotted by the symbol '●') or a pair of the branches 'b_1' and 'b_2' (plotted by the symbol '●') appeared as a single-mode solution. Namely, it was observe that the single-mode solution occurred either in tank 1 or in tank 2, just as predicted in Fig. 3. It can be seen from Fig. 13 that the theoretical curves agree well with the experimental data. It was demonstrated by a comparison between Figs. 12 and 13 that the TLD with two tanks showed less vibration suppression than the TLD with a single tank, because single-mode solutions 'a_1' and 'b_2' occurred in Fig. 13(a).

Fig. 14 shows the photos of the movement of the liquid surfaces, which were taken at $f = 5.45$ Hz in Fig. 13 from the camera eye in the side view. Figs. 14(a) and (b) instantiate a single-mode solution which occurred in tanks 1 and 2, respectively. Fig. 14(c) instantiates a double-mode solution which occurred in both tanks. The elevations η_1^* and η_2^* of the liquid surfaces were in phase in Fig. 14(c). We also observed the type of the anti-phase liquid elevations which were predicted in Fig. 4(d).

Fig. 15 shows a comparison between the theoretical and experimental frequency response curves for apparatus C carrying the two tanks with different liquid levels when $h_1^*/l^* = 0.60$ and $h_2^*/l^* = 0.55$. This figure was similar to Fig. 13, except that the left boundary points of the double-mode solutions 'c_1' and 'c_2' change saddle-node bifurcation points from pitchfork bifurcation points.

Fig. 16 shows a comparison between the theoretical and experimental frequency response curves for apparatus D, where only the mass m of the structure was increased from the case for apparatus B, to investigate the influence of the mistuning. Therefore, the natural frequency p_0 in this apparatus was smaller

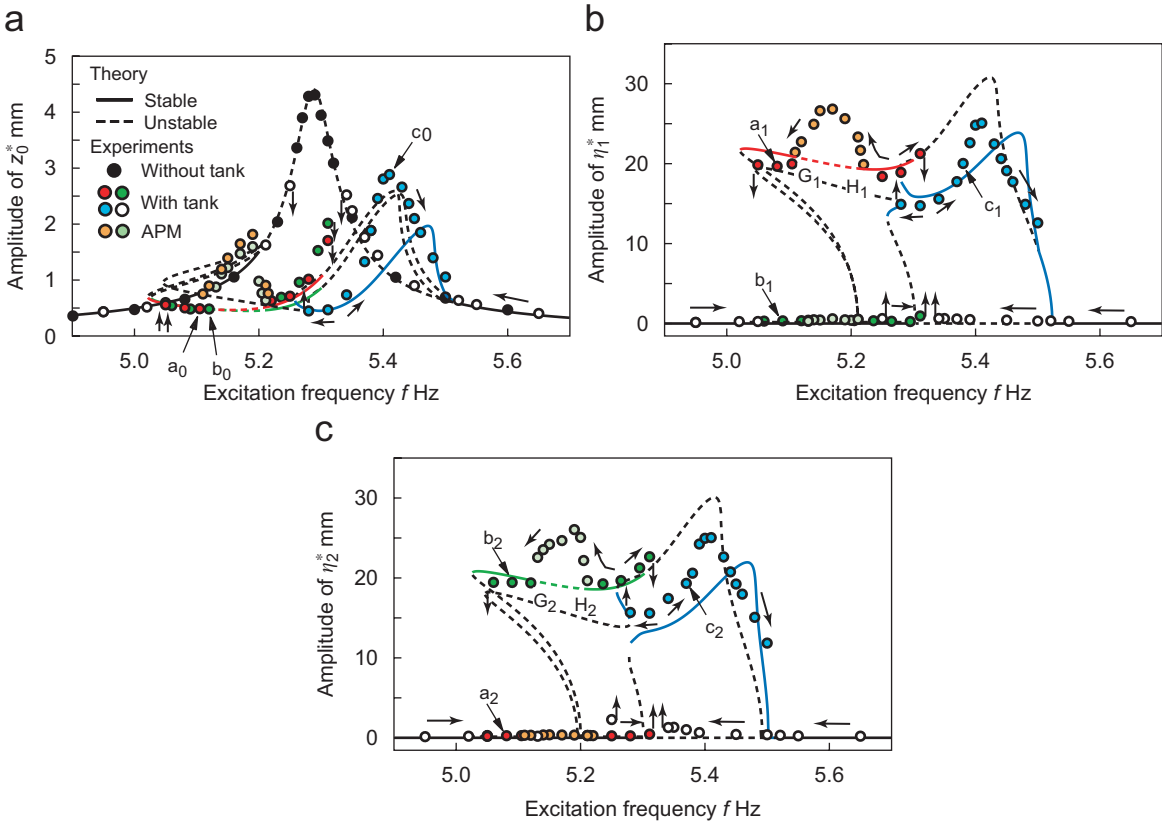

Fig. 16. A comparison between the theoretical and experimental frequency response curves for apparatus D when $h_1^*/l^* = 0.6$, $h_2^*/l^* = 0.55$, $\sigma_1 = -0.170$ Hz and $\bar{\sigma}_1 = -0.124$ Hz (i.e., $\sigma_1/p_1 = -0.062$, $\bar{\sigma}_1/p_1 = -0.045$): (a) amplitudes of z_0^*; (b) amplitudes of η_1^*; (c) amplitudes of η_2^*.

than that in apparatus B. Thus, it is found from Table 1 that the relationship $p_0 \cong 2p_1 \cong 2\bar{p}_1$ was not satisfied precisely, because $\sigma_1 = -0.170$ Hz and $\bar{\sigma}_1 = -0.124$ Hz (i.e., $\sigma_1/p_1 = -0.062$, $\bar{\sigma}_1/p_1 = -0.045$ in dimensionless expression). The new peaks appeared on the branches corresponding to the single-mode solutions, as plotted by the symbols '●' and '●'.

The time histories were observed at $f = 5.12$ Hz, $f = 5.15$ Hz and 5.17 Hz in apparatus D, as shown in Figs. 17(a)–(c), respectively. It was found that the system encountered the APM motion at the intervals G_1H_1 and G_2H_2. As the excitation frequency increased, the system encountered a period-one solution shown in Fig. 17(a), and then twice in Fig. 17(b). Finally, the amplitude changed irregularly in Fig. 17(c) and this exhibits a chaotic vibration.

Fig. 18 shows a comparison between the theoretical and experimental frequency response curves for apparatus E carrying the two tanks with lower liquid levels when $h_1^*/l^* = h_2^*/l^* = 0.258$. It was instantiated by the experiments that the single-mode solution, as shown by the branches 'a_1' or 'b_2', appeared on the right side of the response curve. However, there is a large discrepancy between the theoretical and experimental results in Fig. 18. As explained by Faltinsen et al. for sway/roll excitations [14], this discrepancy may indicate inapplicability of the modal equations based on Eq. (15). The reason is due to internal (secondary) resonances and the shallowness of the fluid flow.

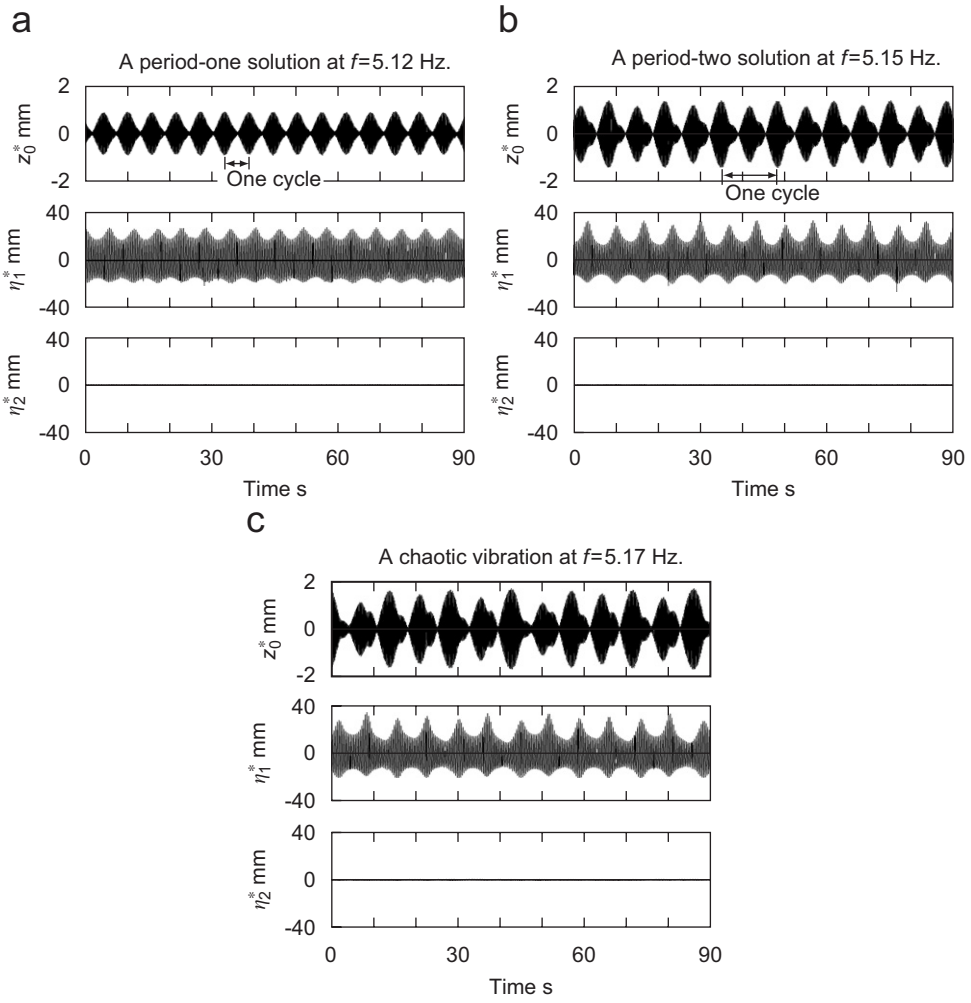

Fig. 17. Time histories for amplitude- and phase-modulated motion obtained in Fig. 16: (a) a period-one solution at $f = 5.12$ Hz; (b) a period-two solution at $f = 5.15$ Hz; (c) a chaotic vibration at $f = 5.17$ Hz.

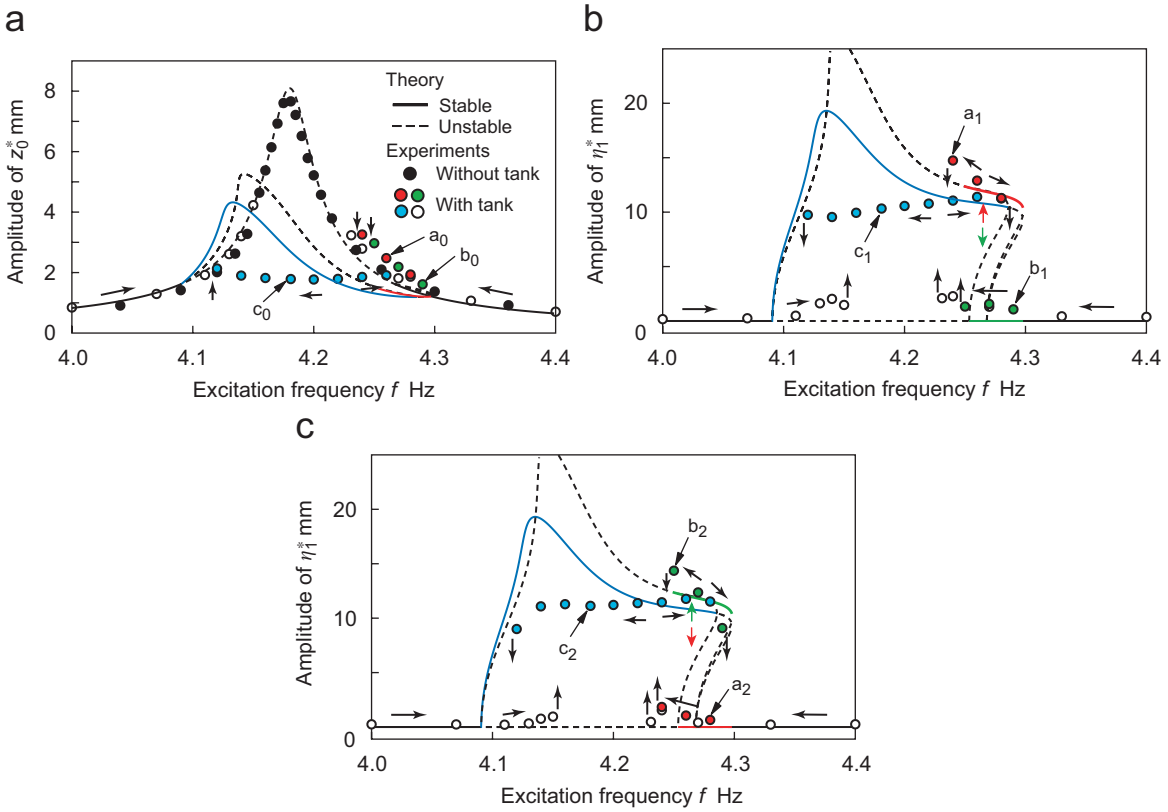

Fig. 18. A comparison between the theoretical and experimental frequency response curves for apparatus E when $h_1^*/l^* = h_2^*/l^* = 0.258$: (a) amplitudes of z_0^*; (b) amplitudes of η_1^*; (c) amplitudes of η_2^*.

6. Conclusions

When the elastic structure carrying two rectangular liquid-filled tanks is subjected to vertical harmonic excitation, the autoparametric resonances of the structure and sloshing are investigated. The results are summarized as follows:

(1) Harmonic oscillations in the structure and 1/2-oder subharmonic oscillations in sloshing in the two tanks appear when the natural frequency ratio 2:1:1 is approximately satisfied.
(2) A single-mode solution in either tank and a double-mode solution in both tanks occur depending on the excitation frequency.
(3) As the liquid level decreases, the region of the single-mode solution moves from the left side of the frequency response curve, to both sides then to the right side, along with the excitation frequency.
(4) When the internal resonance ratio is not satisfied precisely, Hopf bifurcations appear on the branch of the response curve corresponding to the single-mode solution, and the amplitude- and phase-modulated motions including chaotic vibrations may occur. This phenomenon affects the performance of TLDs.
(5) Experimental results confirm the validity of the theoretical analysis except for lower liquid levels. There was a comparatively large discrepancy between the theoretical and experimental results for lower liquid levels. The reason may imply the less validity of the assumption of ordering and the shallowness of the fluid flow.
(6) The simple modal method of the theoretical analysis is proposed to show the comparison of the theoretical results with the experimental data. More precise method should be developed especially for lower liquid

levels by using a shallow water wave theory. Furthermore, TLDs for horizontal sinusoidal excitation as well as random excitation should be also investigated considering the effect of the nonlinear hydrodynamic force.

Acknowledgments

The author would like to thank one of the referees for the many valuable comments and the information about the many references to the manuscript.

Appendix A. Nonlinear terms in Eq. (16)

The nonlinear terms H_j ($j = 1,2,\ldots,7$) in Eq. (16) are given by

$$\begin{aligned}
H_1\left(\ddot{z}_0,\dot{b}_1,\dot{\bar{b}}_1,b_1,\bar{b}_1\right) &= S_1(1+\psi_1\ddot{z}_0)b_1^2 + S_2\dot{b}_1^2 + S_3(1+\psi_1\ddot{z}_0)\bar{b}_1^2 + S_4\dot{\bar{b}}_1^2,\\
H_2(\dot{b}_i,b_i) &= S_5\dot{b}_1\dot{b}_2 + S_6 b_1\dot{b}_1^2 + S_7 b_1 b_2 + S_8 b_1^3,\\
H_3(\ddot{z}_0,\dot{b}_i,b_i) &= S_9(1+\psi_1\ddot{z}_0)b_1^2 + S_{10}\dot{b}_1^2 + S_{11}\dot{b}_1\dot{b}_3 + S_{12}b_1 b_3,\\
H_4(\dot{b}_i,b_i) &= S_{13}\dot{b}_1\dot{b}_2 + S_{14}b_1\dot{b}_1^2 + S_{15}b_1 b_2 + S_{16}b_1^3,\\
H_5\left(\dot{\bar{b}}_i,\bar{b}_i\right) &= S_{17}\dot{\bar{b}}_1\dot{\bar{b}}_2 + S_{18}\bar{b}_1\dot{\bar{b}}_1^2 + S_{19}\bar{b}_1\bar{b}_2 + S_{20}\bar{b}_1^3,\\
H_6\left(\ddot{z}_0,\dot{\bar{b}}_i,\bar{b}_i\right) &= S_{21}(1+\psi_1\ddot{z}_0)\bar{b}_1^2 + S_{22}\dot{\bar{b}}_1^2 + S_{23}\dot{\bar{b}}_1\dot{\bar{b}}_3 + S_{24}\bar{b}_1\bar{b}_3,\\
H_7\left(\dot{\bar{b}}_i,\bar{b}_i\right) &= S_{25}\dot{\bar{b}}_1\dot{\bar{b}}_2 + S_{26}\bar{b}_1\dot{\bar{b}}_1^2 + S_{27}\bar{b}_1\bar{b}_2 + S_{28}\bar{b}_1^3,
\end{aligned} \tag{A.1}$$

where S_k ($k = 1,\ 2,\ldots,28$) are all constants determined by the system parameters, and they are given as follows:

$$\begin{aligned}
&S_1 = -Q_{37}/\psi_1,\ \ S_2 = Q_{38}/\psi_1^2,\ \ S_3 = -Q_{39}/\psi_1,\ \ S_4 = Q_{40}\Big/\bar{\psi}_1^2,\ \ S_5 = Q_{11}/\psi_1 + (Q_9+Q_{12})/\psi_2,\\
&S_6 = (Q_{10}+2Q_{13}-Q_7Q_{16})/\psi_1 - Q_{12}Q_{16}/\psi_1^2 + Q_{18}(Q_9+Q_{12})/(\psi_1\psi_2),\\
&S_7 = -Q_6-Q_7-(Q_{11}+Q_{12})/\psi_1,\ \ S_8 = Q_6Q_7 - Q_8 + (Q_6Q_{12}-Q_{13})/\psi_1,\\
&S_9 = -(\psi_2Q_6+Q_{18})/\psi_1,\ \ S_{10} = (\psi_2Q_{16}+\psi_1Q_{18})/\psi_1^2,\ \ S_{11} = (\psi_2Q_{17}+\psi_3Q_{19}+\psi_1Q_{20})/(\psi_1\psi_3),\\
&S_{12} = \{\psi_2(Q_6-Q_{15})-Q_{19}-Q_{20}\}/\psi_1,\ \ S_{13} = (\psi_3Q_{22}+\psi_2Q_{23}+\psi_1Q_{24})/(\psi_1\psi_2),\\
&S_{14} = 2Q_{25}/\psi_1 + Q_{16}(\psi_3Q_7-Q_{24})/\psi_1^2 + Q_{18}(\psi_3Q_{22}+\psi_1Q_{24})/(\psi_1^2\psi_2),\\
&S_{15} = \{\psi_3(Q_6+Q_7)-Q_{23}-Q_{24}\}/\psi_1,\ \ S_{16} = \{Q_6Q_{24}-Q_{25}-\psi_3(Q_6Q_7+Q_{21})\}/\psi_1,\\
&S_{17} = Q_{11}/\bar{\psi}_1 + (Q_{28}+Q_{12})/\bar{\psi}_2,\\
&S_{18} = (Q_{29}+2Q_{30}-Q_{27}Q_{33})/\bar{\psi}_1 - Q_{12}Q_{33}\Big/\bar{\psi}_1^2 + Q_{18}(Q_{28}+Q_{12})/(\bar{\psi}_1\bar{\psi}_2),\\
&S_{19} = -\{\bar{\psi}_1(Q_{26}+Q_{27})+Q_{11}+Q_{12}\}/\psi_1,\ \ S_{20} = \{\bar{\psi}_1(Q_{26}Q_{27}-Q_8)+Q_{12}Q_{26}-Q_{30}\}/\psi_1,\\
&S_{21} = -(\bar{\psi}_2Q_{26}+Q_{18})/\psi_1,\ \ S_{22} = (\bar{\psi}_2Q_{33}+\bar{\psi}_1Q_{18})\Big/\bar{\psi}_1^2,\ \ S_{23} = (\bar{\psi}_2Q_{34}+\bar{\psi}_3Q_{19}+\bar{\psi}_1Q_{20})/(\bar{\psi}_1\bar{\psi}_3),\\
&S_{24} = \{\bar{\psi}_2(Q_{26}-Q_{32})-Q_{19}-Q_{20}\}/\psi_1,\ \ S_{25} = (\bar{\psi}_3Q_{35}+\bar{\psi}_2Q_{23}+\bar{\psi}_1Q_{24})/(\bar{\psi}_1\bar{\psi}_2),\\
&S_{26} = 2Q_{36}/\bar{\psi}_1 + Q_{33}(\bar{\psi}_3Q_{27}-Q_{24})\Big/\bar{\psi}_1^2 + Q_{18}(\bar{\psi}_3Q_{35}+\bar{\psi}_1Q_{24})\Big/(\bar{\psi}_1^2\bar{\psi}_2),\\
&S_{27} = \{\bar{\psi}_3(Q_{26}+Q_{27})-Q_{23}-Q_{24}\}/\psi_1,\ \ S_{28} = \{Q_{26}Q_{24}-Q_{36}-\bar{\psi}_3(Q_{26}Q_{27}+Q_{21})\}/\psi_1,
\end{aligned} \tag{A.2}$$

where Q_l ($l = 1, 2, \ldots, 40$) are given as follows:

$$
\begin{aligned}
&Q_1 = v + d_1h_1 + d_2h_2,\ Q_2 = -d_1,\ Q_3 = -\frac{\lambda_1^2 d_1}{4\cosh^2(\lambda_1 h_1)},\ Q_4 = -d_2,\ Q_5 = -\frac{\lambda_1^2 d_2}{4\cosh^2(\lambda_1 h_2)},\\
&Q_6 = -\tfrac{1}{2}\psi_1,\ Q_7 = -\tfrac{1}{2}\psi_2,\ Q_8 = \tfrac{3}{8}\lambda_1^2,\ Q_9 = -\tfrac{1}{2}(\lambda_1\lambda_2 + \psi_1\psi_2),\ Q_{10} = \lambda_1^2\psi_1,\\
&Q_{11} = \tfrac{1}{2}\lambda_1(\lambda_1 - \lambda_2),\ Q_{12} = -\tfrac{1}{2}\lambda_2(\lambda_1 - \lambda_2),\ Q_{13} = -\tfrac{1}{8}\lambda_1^2\psi_1,\ Q_{14} = \tfrac{1}{4}(\lambda_1^2 + \psi_1^2),\ Q_{15} = \tfrac{1}{2}\psi_3,\\
&Q_{16} = \tfrac{1}{4}(\lambda_1^2 - \psi_1^2),\ Q_{17} = \tfrac{1}{2}(\lambda_1\lambda_3 + \psi_1\psi_3),\ Q_{18} = \lambda_1^2,\ Q_{19} = -\tfrac{1}{2}\lambda_1(\lambda_1 - \lambda_3),\\
&Q_{20} = \tfrac{1}{2}\lambda_3(\lambda_1 - \lambda_3),\ Q_{21} = -\tfrac{1}{8}\lambda_1^2,\ Q_{22} = -\tfrac{1}{2}(\lambda_1\lambda_2 - \psi_1\psi_2),\ Q_{23} = -\tfrac{1}{2}\lambda_1(\lambda_1 + \lambda_2),\\
&Q_{24} = -\tfrac{1}{2}\lambda_2(\lambda_1 + \lambda_2),\ Q_{25} = \tfrac{3}{8}\lambda_1^2\psi_1,\ Q_{26} = -\tfrac{1}{2}\bar{\psi}_1,\ Q_{27} = -\tfrac{1}{2}\bar{\psi}_2,\ Q_{28} = -\tfrac{1}{2}(\lambda_1\lambda_2 + \bar{\psi}_1\bar{\psi}_2),\\
&Q_{29} = \lambda_1^2\bar{\psi}_1,\ Q_{30} = -\tfrac{1}{8}\lambda_1^2\bar{\psi}_1,\ Q_{31} = \tfrac{1}{4}(\lambda_1^2 + \bar{\psi}_1^2),\ Q_{32} = \tfrac{1}{2}\bar{\psi}_3,\ Q_{33} = \tfrac{1}{4}(\lambda_1^2 - \bar{\psi}_1^2),\\
&Q_{34} = \tfrac{1}{2}(\lambda_1\lambda_3 + \bar{\psi}_1\bar{\psi}_3),\ Q_{35} = -\tfrac{1}{2}(\lambda_1\lambda_2 - \bar{\psi}_1\bar{\psi}_2),\ Q_{36} = \tfrac{3}{8}\lambda_1^2\bar{\psi}_1,\\
&Q_{37} = Q_2Q_6,\ Q_{38} = Q_3 - Q_2Q_{14},\ Q_{39} = Q_4Q_{26},\ Q_{40} = Q_5 - Q_4Q_{31},\\
&\psi_n = \lambda_n \tanh(\lambda_n h_1),\ \bar{\psi}_n = \lambda_n \tanh(\lambda_n h_2).
\end{aligned}
\tag{A.3}
$$

Appendix B. The ordinary differential equations for a_0, $\bar{a}_0$, a_n, b_n, $\bar{a}_n$ and $\bar{b}_n$

Modal equations for tank 1 is given within the accuracy of $O(\varepsilon)$ by

$$
\begin{aligned}
&\dot{a}_1 + \left(\frac{1}{\psi_1} + \ddot{z}_0\right)b_1 + Q_6\dot{a}_1b_2 + Q_7\dot{a}_2b_1 + Q_8\dot{a}_1b_1^2 + Q_9a_1a_2 + Q_{10}a_1^2b_1 = 0,\\
&\dot{b}_1 - \psi_1a_1 + Q_{11}a_1b_2 + Q_{12}a_2b_1 + Q_{13}a_1b_1^2 = 0,\\
&\dot{a}_0 - Q_6\dot{a}_1b_1 + Q_{14}a_1^2 = 0,\\
&\dot{a}_2 + \left(\frac{1}{\psi_1} + \ddot{z}_0\right)b_2 + Q_6\dot{a}_1b_1 - Q_6\dot{a}_1b_3 + Q_{15}\dot{a}_3b_1 + Q_{16}a_1^2 + Q_{17}a_1a_3 = 0,\\
&\dot{b}_2 - \psi_2a_2 + Q_{18}a_1b_1 + Q_{19}a_1b_3 + Q_{20}a_3b_1 = 0,\\
&\dot{a}_3 + \left(\frac{1}{\psi_1} + \ddot{z}_0\right)b_3 - Q_6\dot{a}_1b_2 - Q_7\dot{a}_2b_1 + Q_{21}\dot{a}_1b_1^2 + Q_{22}a_1a_2 = 0,\\
&\dot{b}_3 - \psi_3a_3 + Q_{23}a_1b_2 + Q_{24}a_2b_1 + Q_{25}a_1b_1^2 = 0.
\end{aligned}
\tag{B.1a–g}
$$

Modal equations for tank 2 is given within the accuracy of $O(\varepsilon)$ by

$$
\begin{aligned}
&\dot{\bar{a}}_1 + \left(\frac{1}{\psi_1} + \ddot{z}_0\right)\bar{b}_1 + Q_{26}\dot{\bar{a}}_1\bar{b}_2 + Q_{27}\dot{\bar{a}}_2\bar{b}_1 + Q_8\dot{\bar{a}}_1\bar{b}_1^2 + Q_{28}\bar{a}_1\bar{a}_2 + Q_{29}\bar{a}_1^2\bar{b}_1 = 0,\\
&\dot{\bar{b}}_1 - \bar{\psi}_1\bar{a}_1 + Q_{11}\bar{a}_1\bar{b}_2 + Q_{12}\bar{a}_2\bar{b}_1 + Q_{30}\bar{a}_1\bar{b}_1^2 = 0,\\
&\dot{\bar{a}}_0 - Q_{26}\dot{\bar{a}}_1\bar{b}_1 + Q_{31}\bar{a}_1^2 = 0,\\
&\dot{\bar{a}}_2 + \left(\frac{1}{\psi_1} + \ddot{z}_0\right)\bar{b}_2 + Q_{26}\dot{\bar{a}}_1\bar{b}_1 - Q_{26}\dot{\bar{a}}_1\bar{b}_3 + Q_{32}\dot{\bar{a}}_3\bar{b}_1 + Q_{33}\bar{a}_1^2 + Q_{34}\bar{a}_1\bar{a}_3 = 0,\\
&\dot{\bar{b}}_2 - \bar{\psi}_2\bar{a}_2 + Q_{18}\bar{a}_1\bar{b}_1 + Q_{19}\bar{a}_1\bar{b}_3 + Q_{20}\bar{a}_3\bar{b}_1 = 0,\\
&\dot{\bar{a}}_3 + \left(\frac{1}{\psi_1} + \ddot{z}_0\right)\bar{b}_3 - Q_{26}\dot{\bar{a}}_1\bar{b}_2 - Q_{27}\dot{\bar{a}}_2\bar{b}_1 + Q_{21}\dot{\bar{a}}_1\bar{b}_1^2 + Q_{35}\bar{a}_1\bar{a}_2 = 0,\\
&\dot{\bar{b}}_3 - \bar{\psi}_3\bar{a}_3 + Q_{23}\bar{a}_1\bar{b}_2 + Q_{24}\bar{a}_2\bar{b}_1 + Q_{36}\bar{a}_1\bar{b}_1^2 = 0.
\end{aligned}
\tag{B.2a–g}
$$

Then Eqs. (b), (e) and (g) in Eqs. (B.1) and (B.2) lead to

$$
a_1 \cong \frac{\dot{b}_1}{\psi_1} + \frac{1}{\psi_1^2}\left(Q_{11}\dot{b}_1b_2 + \frac{\psi_1}{\psi_2}Q_{12}b_1\dot{b}_2\right) + \frac{1}{\psi_1^2}\left(Q_{13} + \frac{1}{\psi_2}Q_{12}Q_{18}\right)b_1^2\dot{b}_1,
$$

$$a_2 \cong \frac{\dot{b}_2}{\psi_2}+\frac{1}{\psi_1\psi_2}\left(Q_{18}\dot{b}_1b_1+Q_{19}\dot{b}_1b_3\right)+\frac{Q_{20}}{\psi_2\psi_3}b_1\dot{b}_3,$$
$$a_3 \cong \frac{\dot{b}_3}{\psi_3}+\frac{1}{\psi_3}\left(\frac{Q_{23}}{\psi_1}\dot{b}_1b_2+\frac{Q_{24}}{\psi_2}b_1\dot{b}_2\right)+\frac{1}{\psi_1\psi_3}\left(Q_{25}+\frac{1}{\psi_2}Q_{18}Q_{24}\right)b_1^2\dot{b}_1. \tag{B.3}$$

and

$$\bar{a}_1 \cong \frac{\dot{\bar{b}}_1}{\bar{\psi}_1}+\frac{1}{\bar{\psi}_1^2}\left(Q_{11}\dot{\bar{b}}_1\bar{b}_2+\frac{\bar{\psi}_1}{\bar{\psi}_2}Q_{12}\bar{b}_1\dot{\bar{b}}_2\right)+\frac{1}{\bar{\psi}_1^2}\left(Q_{13}+\frac{1}{\bar{\psi}_2}Q_{12}Q_{18}\right)\bar{b}_1^2\dot{\bar{b}}_1,$$
$$\bar{a}_2 \cong \frac{\dot{\bar{b}}_2}{\bar{\psi}_2}+\frac{1}{\bar{\psi}_1\bar{\psi}_2}\left(Q_{18}\dot{\bar{b}}_1\bar{b}_1+Q_{19}\dot{\bar{b}}_1\bar{b}_3\right)+\frac{Q_{20}}{\bar{\psi}_2\bar{\psi}_3}\bar{b}_1\dot{\bar{b}}_3,$$
$$\bar{a}_3 \cong \frac{\dot{\bar{b}}_3}{\bar{\psi}_3}+\frac{1}{\bar{\psi}_3}\left(\frac{Q_{23}}{\bar{\psi}_1}\dot{\bar{b}}_1\bar{b}_2+\frac{Q_{24}}{\bar{\psi}_2}\bar{b}_1\dot{\bar{b}}_2\right)+\frac{1}{\bar{\psi}_1\bar{\psi}_3}\left(Q_{36}+\frac{1}{\bar{\psi}_2}Q_{18}Q_{24}\right)\bar{b}_1^2\dot{\bar{b}}. \tag{B.4}$$

Also, Eqs. (a), (d) and (f) in Eqs. (B.1) and (B.2) lead to

$$\begin{aligned}\dot{a}_1 \cong & -\left(\frac{1}{\psi_1}+\ddot{z}_0\right)b_1-\frac{Q_9}{\psi_1\psi_2}\dot{b}_1\dot{b}_2+\frac{1}{\psi_1^2}\left(-Q_{10}+Q_7Q_{16}-\frac{1}{\psi_2}Q_9Q_{18}\right)b_1\dot{b}_1^2\\ & +\frac{1}{\psi_1}(Q_6+Q_7)b_1b_2+\frac{1}{\psi_1}(Q_8-Q_6Q_7)b_1^3,\\ \dot{a}_2 \cong & -\left(\frac{1}{\psi_1}+\ddot{z}_0\right)b_2+Q_6\left(\frac{1}{\psi_1}+\ddot{z}_0\right)b_1^2-\frac{Q_{16}}{\psi_1^2}\dot{b}_1^2-\frac{Q_{17}}{\psi_1\psi_3}\dot{b}_1\dot{b}_3+\frac{1}{\psi_1}(Q_{15}-Q_6)b_1b_3,\\ \dot{a}_3 \cong & -\left(\frac{1}{\psi_1}+\ddot{z}_0\right)b_3-\frac{Q_{22}}{\psi_1\psi_2}\dot{b}_1\dot{b}_2-\frac{1}{\psi_1^2}\left(Q_7Q_{16}+\frac{1}{\psi_2}Q_{18}Q_{22}\right)b_1\dot{b}_1^2\\ & -\frac{1}{\psi_1}(Q_6+Q_7)b_1b_2+\frac{1}{\psi_1}(Q_6Q_7+Q_{21})b_1^3\end{aligned} \tag{B.5}$$

and

$$\begin{aligned}\dot{\bar{a}}_1 \cong & -\left(\frac{1}{\psi_1}+\ddot{z}_0\right)\bar{b}_1-\frac{Q_{28}}{\bar{\psi}_1\bar{\psi}_2}\dot{\bar{b}}_1\dot{\bar{b}}_2+\frac{1}{\bar{\psi}_1^2}\left(-Q_{29}+Q_{27}Q_{33}-\frac{1}{\bar{\psi}_2}Q_{28}Q_{18}\right)\bar{b}_1\dot{\bar{b}}_1^2\\ & +\frac{1}{\psi_1}(Q_{26}+Q_{27})\bar{b}_1\bar{b}_2+\frac{1}{\psi_1}(Q_8-Q_{26}Q_{27})\bar{b}_1^3,\\ \dot{\bar{a}}_2 \cong & -\left(\frac{1}{\psi_1}+\ddot{z}_0\right)\bar{b}_2+Q_{26}\left(\frac{1}{\psi_1}+\ddot{z}_0\right)\bar{b}_1^2-\frac{Q_{33}}{\bar{\psi}_1^2}\dot{\bar{b}}_1^2-\frac{Q_{34}}{\bar{\psi}_1\bar{\psi}_3}\dot{\bar{b}}_1\dot{\bar{b}}_3+\frac{1}{\psi_1}(Q_{32}-Q_{26})\bar{b}_1\bar{b}_3,\\ \dot{\bar{a}}_3 \cong & -\left(\frac{1}{\psi_1}+\ddot{z}_0\right)\bar{b}_3-\frac{Q_{35}}{\bar{\psi}_1\bar{\psi}_2}\dot{\bar{b}}_1\dot{\bar{b}}_2-\frac{1}{\bar{\psi}_1^2}\left(Q_{27}Q_{33}+\frac{1}{\psi_2}Q_{18}Q_{35}\right)\bar{b}_1\dot{\bar{b}}_1^2\\ & -\frac{1}{\psi_1}(Q_{26}+Q_{27})\bar{b}_1\bar{b}_2+\frac{1}{\psi_1}(Q_{26}Q_{27}+Q_{21})\bar{b}_1^3.\end{aligned} \tag{B.6}$$

Differentiating Eq. (b), (e) and (g) in Eqs. (B.1) and (B.2) with respect to time, and then substituting Eqs. (B.3)–(B.6) into the resulting equations, one can obtain the modal equations for sloshing given by Eqs. (16b) and (16c).

Appendix C. Natural frequency of three-dimensional waves

The natural frequencies of the three-dimensional waves with mode (m, n) are given by [8]

$$p_{mn}=\sqrt{g\lambda_{mn}^*\tanh(\lambda_{mn}^*h^*)}\quad(\lambda_{mn}^*=\pi\sqrt{(m/l^*)^2+(n/d^*)^2}). \tag{C.1}$$

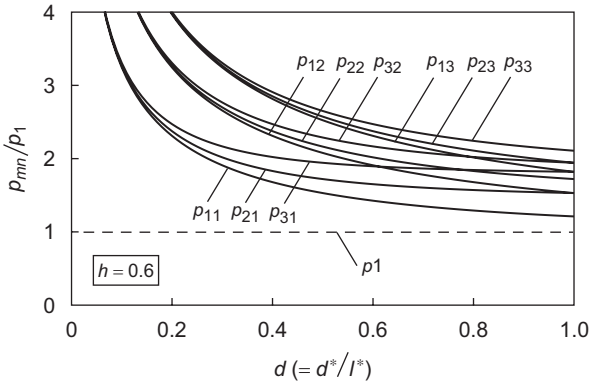

Fig. C1. Natural frequencies p_{mn} of the three-dimensional waves with mode (m, n) showing the influence of the tank width $d(= d^*/l^*)$ for $h = 0.6$.

The corresponding nondimensional natural frequencies, which are normalized by the natural frequency of the first sloshing mode $p_1 = \sqrt{g\lambda_1^* \tanh(\lambda_1^* h^*)}$ $(\lambda_1^* = \pi/l^*)$, are

$$p_{mn}/p_1 = \sqrt{\kappa_{mn} \tanh(\pi\kappa_{mn}h)/\tanh(\pi h)} \quad \left(\kappa_{mn} = \pi\sqrt{m^2 + (n/d)^2}\right). \tag{C.2}$$

Fig. C1 shows the values of p_{mn}/p_1 for $h = 0.6$. The horizontal broken line, $p_{mn}/p_1 = 1$, corresponds to the natural frequency p_1. If the value of the tank width $d(= d^*/l^*)$ is less than 0.2, the natural frequencies p_{mn} are all larger than double the natural frequency p_1. This is true even for $h < 0.6$. Therefore, three-dimensional waves never occur for the values of the system parameters discussed here.

References

[1] R.A. Ibrahim, *Liquid Sloshing Dynamics*, Cambridge University Press, Cambridge, 2005.
[2] K. Senda, N. Nakagawa, On the vibration of an elevated water-tank—I, *Technical Reports of Osaka University* 4 (117) (1954) 247–264.
[3] R.E. Hutton, An investigation of resonant, nonlinear, nonplanar free surface oscillations of a fluid. *NASA Technical Note D-1870,* 1963, pp. 1–64.
[4] H.N. Abramson, The dynamic behavior of liquids in moving containers, *NASA SP-106*, 1966.
[5] R. Skalak, M.I. Yarymovych, Forced large amplitude surface waves, *Proceedings of the Fourth US National Congress on Applied Mechanics*, 1962, pp. 1411–1418.
[6] F.G. Dodge, D.D. Kana, H.N. Abramson, Liquid surface oscillations in longitudinal excited rigid cylindrical containers, *AIAA Journal* 3 (4) (1965) 685–695.
[7] M. Faraday, On a peculiar class of acoustical figures, and on certain forms assumed by groups of particles upon vibrating elastic surfaces, *Philosophical Transactions on the Royal Society of London* 121 (1831) 299–340.
[8] D.M. Henderson, J.W. Miles, Faraday waves in 2:1 internal resonance, *Journal of Fluid Mechanics* 222 (1991) 449–470.
[9] J.W. Miles, On Faraday waves, *Journal of Fluid Mechanics* 248 (1993) 671–683.
[10] J.W. Miles, Faraday waves: rolls versus squares, *Journal of Fluid Mechanics* 269 (1994) 353–371.
[11] D. Fultz, An experimental note on finite-amplitude standing gravity waves, *Journal of Fluid Mechanics* 13 (1962) 193–212.
[12] J.R. Ockendon, H. Ockendon, Resonant surface waves, *Journal of Fluid Mechanics* 59 (1973) 397–413.
[13] S. Hayama, K. Aruga, T. Watanabe, Nonlinear response of sloshing in rectangular tanks (1st report, nonlinear response of surface elevation), *Bulletin of the JSME* 26 (219) (1983) 1641–1648.
[14] O.M. Faltinsen, O.F. Rognebakke, I.A. Lukovsky, A.N. Timokha, Multidimensional modal analysis of nonlinear sloshing in a rectangular tank with finite water depth, *Journal of Fluid Mechanics* 407 (2000) 201–234.
[15] D.D. Waterhouse, Resonant sloshing near a critical depth, *Journal of Fluid Mechanics* 28 (1994) 313–318.
[16] O.M. Faltinsen, A.N. Timokha, Asymptotic modal approximation of nonlinear resonant sloshing in a rectangular tank with small fluid depth, *Journal of Fluid Mechanics* 470 (2002) 319–357.
[17] D.F. Hill, Transient and steady-state amplitudes of forces waves in rectangular tanks, *Physics of Fluids* 15 (6) (2003) 1576–1587.
[18] D.F. Hill, J. Frandsen, Transient evolution of weakly nonlinear sloshing waves: an analytical and numerical comparison, *Journal of Engineering Mathematics* 58 (2) (2005) 187–198.

[19] H. Bredmose, M. Brocchini, D.H. Peregrine, L. Thais, Experimental investigation and numerical modeling of steep forced water waves, *Journal of Fluid Mechanics* 490 (2003) 217–249.
[20] V.J. Modi, F. Welt, Vibration control using nutation dampers, *Proceedings of the International Conference on Flow Induced Vibrations*, Bowness-on-Windermere, England, 1987, pp. 369–376.
[21] Y. Fujino, M. Pacheco, L.-M. Sun, P. Chaiseri, M. Isobe, Simulation of nonlinear Wave in rectangular tuned liquid damper (TLD) and its verification, *Transactions of the Japan Society of Civil Engineers* A-35 (1989) 561–574 (in Japanese).
[22] H. Hagiuda, Oscillation control system exploiting fluid force generated by water sloshing, *Mitsui Zosen Technical Review* 137 (1988) 13–20 (in Japanese).
[23] Y. Tamura, K. Fujii, T. Ohtsuki, T. Wakahara, R. Kohsaka, Effectiveness of tuned liquid dampers under wind excitation, *Engineering Structures* 17 (9) (1995) 609–621.
[24] T. Ikeda, N. Nakagawa, Non-linear vibrations of a structure caused by water sloshing in a rectangular tank, *Journal of Sound and Vibration* 201 (1) (1997) 23–41.
[25] T. Ikeda, T. Hirayama, N. Nakagawa, Nonlinear vibrations of a structure caused by water sloshing in a cylindrical tank, *Transactions of the JSME, International Journal, Series C* 41 (3) (1998) 639–651.
[26] S. Kaneko, O. Yoshida, Modeling of deepwater-type rectangular tuned liquid damper with submerged nets, *Transaction of the ASME, Journal of Pressure Vessel Technology* 121 (4) (1999) 413–422.
[27] J.B. Fradsen, Numerical predictions of tuned liquid tank structural systems, *Journal of Fluids and Structures* 20 (3) (2005) 309–329.
[28] R.A. Ibrahim, A.D.S. Barr, Autoparametric resonance in a structure containing a liquid, part I: two mode interaction, *Journal of Sound and Vibration* 42 (2) (1975) 159–179.
[29] T. Ikeda, Nonlinear parametric vibrations of an elastic structure with a rectangular liquid tank, *Nonlinear Dynamics* 33 (1) (2003) 43–70.
[30] T. Ikeda, S. Murakami, Autoparametric resonances in a structure/fluid interaction system carrying a cylindrical liquid tank, *Journal of Sound and Vibration* 285 (3) (2005) 517–546.
[31] J.J. Stoker, *Nonlinear Vibrations*, Wiley, New York, 1950.
[32] N.N. Miseev, On the theory of nonlinear vibrations of a liquid of finite volume, *Journal of Applied Mathematics and Mechanics* 22 (1958) 860–872.
[33] A.F. Vakakis, L. Manevitch, Y.V. Mikhlin, V.N. Pilipchuk, A.A. Zevin, *Normal Modes and Localization in Nonlinear Systems*, Wiley, New York, 1996.
[34] A. Vyas, A.K. Bajaj, Dynamics of autoparametric vibration absorbers using multiple pendulums, *Journal of Sound and Vibration* 246 (1) (2001) 115–135.
[35] A. Wolf, J.B. Swift, H.L. Swinney, J.A. Vastano, Determining Lyapunov exponents from a time series, *Physica* 16D (1985) 285–317.